Spatio-temporal variability of daily and weekly precipitation extremes in South America

Shiraj Khan,[1] Gabriel Kuhn,[1] Auroop R. Ganguly,[1] David J. Erickson III,[2] and George Ostrouchov[2]

Received 28 July 2006; revised 24 July 2007; accepted 7 August 2007; published 29 November 2007.

[1] Spatial and temporal variability of precipitation extremes are investigated by utilizing daily observations available at 2.5° gridded fields in South America for the period 1940–2004. All 65 a of data from 1940–2004 are analyzed for spatial variability. The temporal variability is investigated at each spatial grid by utilizing 25-a moving windows from 1965–2004 and visualized through plots of the slope of the regression line in addition to its quality measure (R^2). The Poisson-generalized Pareto (Poisson-GP) model, which is a peaks over threshold (POT) approach, is applied to weekly precipitation maxima residuals based on the 95%-quantile threshold, while daily data are utilized to analyze the number of consecutive daily extremes and daily extremes in a month based on the 99%-quantile threshold. Using the Poisson-GP model, we compute parameters of the GP distribution, return levels (RL) and a new measure called the *precipitation extremes volatility index* (PEVI). The PEVI measures the variability of extremes and is expressed as a ratio of return levels. From 1965–2004, the PEVI shows increasing trends in the Amazon basin except eastern parts, few parts of the Brazilian highlands, north-west Venezuela including Caracas, north Argentina, Uruguay, Rio De Janeiro, São Paulo, Asuncion, and Cayenne. Catingas, few parts of the Brazilian highlands, São Paulo and Cayenne experience increasing number of consecutive 2- and 3-days extremes from 1965–2004. The number of daily extremes, computed for each month, suggest that local extremes occur mostly from December to April with July to October being relatively quiet periods.

Citation: Khan, S., G. Kuhn, A. R. Ganguly, D. J. Erickson III, and G. Ostrouchov (2007), Spatio-temporal variability of daily and weekly precipitation extremes in South America, *Water Resour. Res.*, *43*, W11424, doi:10.1029/2006WR005384.

1. Introduction

[2] Precipitation extremes can have significant impacts on human society, economics, and nature. Flooding is directly associated with precipitation extremes which can cause large number of casualties, loss of property, water-borne disease outbreaks in humans, plants and animals [*Curriero et al.*, 2001], and extensive damage to crops. An understanding of the intensity and frequency of precipitation extremes can be very useful for infrastructure development to prevent flooding and landslides, as well as for water resources and agricultural management. This may help nations and world bodies like the UN to be better prepared for future disasters caused by floods and flash floods. A better understanding of precipitation extremes can help hydrologic scientists and climatologists gain enhanced understanding of precipitation processes driving the extremes and perhaps delineate possible anthropogenic or natural causes.

[3] Previous studies investigated trends and variability of precipitation extremes in many parts of the world in the twentieth century, specifically the United States [*Karl et al.*, 1995; *Groisman et al.*, 1999], India [*Goswami et al.*, 2006], Southeast Asia and the South Pacific [*Manton et al.*, 2001], Australia [*Suppiah and Hennessy*, 1998; *Groisman et al.*, 1999], Europe [*Haylock and Goodess*, 2004], Caribbean [*Peterson et al.*, 2002], Italy [*Brunetti et al.*, 2002], Balkans [*Cavazos*, 2000], Canada, Norway, Russia, China, Mexico [*Groisman et al.*, 1999], Japan [*Iwashima and Yamamoto*, 1993], Sweden [*Hellstrom and Malmgren*, 2004], south-eastern South America [*Carvalho et al.*, 2002], and the state of São Paulo, Brazil [*Liebmann et al.*, 2001]. However, we are not aware of any prior investigations on spatial and temporal variability of precipitation extremes over the entire continent of South America.

[4] Extreme value theory (EVT) has been widely used in hydrology to perform flood frequency analyses by utilizing historical records of precipitation, steamflow and other variables [*Stedinger and Cohn*, 1986]. In recent years, EVT has been applied in multiple disciplines including hydrology [*Katz et al.*, 2002; *Li et al.*, 2005], ecology [*Gaines and Denny*, 1993; *Katz et al.*, 2005], hurricane

[1] Computational Sciences and Engineering Division, Oak Ridge National Laboratory, Oak Ridge, Tennessee, USA.
[2] Computer Science and Mathematics Division, Oak Ridge National Laboratory, Oak Ridge, Tennessee, USA.

0043-1397/07/2006WR005384$09.00

damage [*Katz*, 2002], temperature [*Brown and Katz*, 1995], wind speed [*Palutikof et al.*, 1999], and wildfire sizes [*Schoenberg et al.*, 2003]. The generalized extreme value (GEV) distribution, developed by *Jenkinson* [1955], has been traditionally utilized for modeling precipitation extremes [*Gumbel*, 1958; *Katz et al.*, 2002; *Nadarajah*, 2005]. This approach is also called the block maxima approach since it fits the distribution to the highest values in blocks of equal size, e.g., maximum yearly precipitation. It has some advantages, e.g., its requirements can be met by a simplified summary of data and the block maxima can be assumed to be independent random variables [*Katz et al.*, 2005]. However, the main drawback of the GEV distribution is that it does not utilize all the available information about the upper tail of the distribution, e.g., two highest extreme precipitation events may occur in the same year [*Katz et al.*, 2005]. An alternative approach is to use peaks over threshold (POT) which was originated in hydrology and makes use of all the data available, e.g., all daily precipitation data [*Todorovic and Zelenhasic*, 1970]. The statistical model underlying the POT method consists of (1) Poisson process for the occurrences of extremes over a large threshold and (2) generalized Pareto (GP) distribution (with scale (σ) and shape (ξ) parameters), developed by *Picklands* [1975], for the distribution of excesses over a large threshold. This model is also termed as Poisson-GP model. Recently, the GP distribution has been utilized for modeling threshold excesses from daily precipitation data [*Li et al.*, 2005; *Wilson and Toumi*, 2005]. This study utilizes the Poisson-GP model for investigating the spatial and temporal variability of precipitation extremes at each grid point in South America.

[5] Daily precipitation data is available in 2.5° gridded fields for the period 1940–2004 in South America. The Poisson-GP model assumes the data to be independent and identically distributed (IID) [*Katz et al.*, 2002]. A long-term trend and seasonality in the data violate the assumption of identically distributed data whereas the assumption of independent data is violated if there is temporal dependence in the data [*Gaines and Denny*, 1993]. In order to check the IID assumption for the Poisson-GP model, we consider three different sets of data based on this daily data: daily data itself, weekly maxima, and weekly maxima residuals. Weekly maxima residuals are obtained by subtracting the long term mean of weekly maxima of a particular week, i.e., mean of maximum weekly precipitation across the same week for all years used in the analysis, from weekly maxima of the same week. These data sets are compared to choose the best data using temporal dependence through autocorrelations and seasonal trends. In order to check the quality of the Poisson-GP model, we also compare these data sets using the Poisson property of the occurrences of extremes and quality of the GP distribution. The scale of the data and the need for efficient computations, which can be eventually automated, preclude choosing thresholds based on human judgment. We choose thresholds as 95%-quantile for weekly maxima and weekly maxima residuals and 99%-quantile for the daily data. The thresholds are computed at each grid, hence the extremes can be said to be local in the context of observed precipitation in the particular grid. Spatial variability is investigated for 65 a (1940–2004) and the last 40 a (1965–2004) are also studied for the temporal variability with 25-a moving window, i.e., 1965–1989, 1966–1990,. . ., 1980–2004. The temporal variability is given by the slope of linear trend obtained by fitting a regression line to 16 values from 16 time windows from 1965–2004. We also plot R^2 obtained from the regression line which provides the overall measure of the quality of fitted regression line. We investigate the spatial and temporal variability of thresholds, σ and ξ and their standard errors, 50-a and 200-a return levels (RL), and *precipitation extremes volatility index* (PEVI) which measures the variability of extremes and is defined as a ratio of RLs. This study computes PEVI as the ratio of 200-a and 50-a RLs, where the latter represents a design return level, e.g., the return level used for infrastructure design, while the former represents rarer and more intense extremes. The PEVI represents a measure of surprise if the rarer extremes were to occur. The advantages of PEVI are easy interpretability, computational efficiency and effective visualization through a single parameter at each grid. The temporal variability of thresholds from 1965–2004 also gives an indication about increasing or decreasing trends in precipitation during that period. On the basis of daily data, the spatial and temporal variability of the number of consecutive 2-days and 3-days extremes and the spatial variations of the number of monthly extremes are investigated.

2. Data and Methodology

2.1. Data Availability

[6] The daily precipitation data used in this study was published for Brazil, Venezuela, north Argentina, Paraguay, Uruguay, Suriname and French Guiana from 1940–2004 by *Liebmann and Allured* [2005]. The data was presented in 2.5° gridded fields which were constructed using daily precipitation totals from 7900 stations. The daily precipitation at each point on a 2.5° grid was calculated by averaging daily precipitation from all stations within a radius of 1.875° of the point. The complete description of this data is given by *Liebmann and Allured* [2005]. The spatial variability is investigated for 65 a from 1940–2004 where the percentage of data points available for the analysis at each grid point is shown in Figure 1a. We analyze all those grid points having 14 or more years of data. For the spatial variability from 1940–2004, 223 grid points are analyzed since they have 14 or more years of data. We investigate temporal variability for 40 a from 1965–2004 by considering 25-a moving windows, i.e., 1965–1989, 1966–1990,. . ., 1980–2004. Figure 1b shows the mean percentage of data points, i.e., mean of 16 percentages of data for 16 moving windows from 1965–2004, available for the analysis at each grid point. A total of 216 grid points are analyzed for the temporal variability since they have mean percentage values of 56% or more which is equivalent to 14 or more years of data out of 25 a.

2.2. Methodology

2.2.1. Poisson-GP Model

[7] If $x_1,\ldots, x_n$ be a sequence of IID observations, the Poisson-GP model consists of two components: (i) the sequence of times at which exceedances occur over a large threshold, u, i.e., $x_i > u$ for some i, is governed by a Poisson process; and (ii) the limiting distribution of the excesses over u, i.e., $x_i - u$ for some i, is the GP distribution [*Katz et*

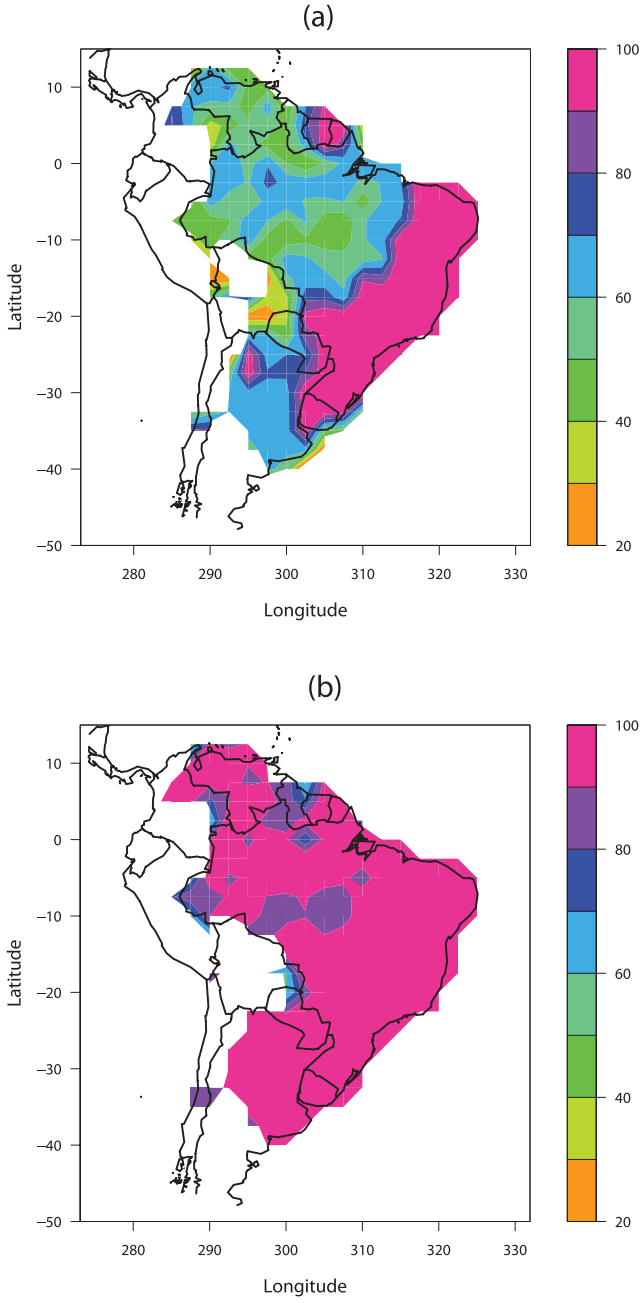

Figure 1. Percentage of total data available at each grid point: (a) Percentage of daily data available in 65 a from 1940–2004; and (b) Mean percentage of daily data available in 40 a from 1965–2004 computed using 25-a moving window from 1965–2004, i.e., 1965–1989, 1966–1990,. . ., 1980–2004. Each grid point having at least 14 a of data is considered for the analysis. This means that all grid points having more than 22% and 56% of data are used for the analysis in (a) and (b), respectively. The white regions on the map indicate either non-availability of data or insufficient data, i.e., less than 14 a of data, for the analysis.

al., 2002]. The first component implies that if threshold exceedances occur independent in time, the time intervals between threshold exceedances, also referred as inter-arrival times of threshold exceedances later in the study, follow one-dimensional *homogeneous Poisson process*. By the definition of one-dimensional *homogeneous Poisson process*, the inter-arrival times of threshold exceedances are independent and exponentially distributed.

[8] Let $x_1,\ldots, x_n$ be a sequence of IID measurements. An extreme event x is defined when it exceeds a threshold u. If $x_{(1)},\ldots, x_{(k)}$ are the k exceedances over threshold u, then threshold excesses are defined as $y_i = x_{(i)} - u$, for $i = 1,\ldots, k$. If $y_1,\ldots, y_k$ is an independent sequence of a random variable, the distribution of these threshold excesses can be approximated by a member of the GP family [*Coles*, 2001]. The cumulative distribution function for the GP is given by

$$F_{\sigma,\xi}(y) = \begin{cases} 1 - [1 + (\xi y/\sigma)]^{-1/\xi}, & 1 + (\xi y/\sigma) > 0, \quad \xi \neq 0 \\ 1 - e^{-y/\sigma}, & \xi = 0, \end{cases} \tag{1}$$

where $y > 0$; $\sigma > 0$ is a scale parameter; and $-\infty < \xi < \infty$ is a shape parameter. The shape parameter is important to understand the qualitative behavior of the GP distribution. The GP distribution has an upper bound for $\xi < 0$ (also called bounded distribution) whereas it is unbounded for $\xi = 0$ (also called light-tailed distribution) and has no upper limit for $\xi > 0$ (also called heavy-tailed distribution) [*Katz et al.*, 2005]. The parameters σ and ξ of the GP distribution are estimated by maximizing the log likelihood function since maximum likelihood estimation assigns the highest probability to the observed data by adopting the model with the greatest likelihood out of all the models under consideration [*Coles*, 2001]. The log likelihood function for the GP distribution defined in equation (1) is given as

$$l_{\sigma,\xi} = \begin{cases} -k\log(\sigma) - (1 + 1/\xi)\sum_{i=1}^{k} \log(c_i), & c_i > 0 \\ -k\log(\sigma) - \frac{1}{\sigma}\sum_{i=1}^{k} y_i, & \xi = 0, \end{cases}$$

where $c_i = (1 + \xi y_i/\sigma)$ [*Coles*, 2001]. The GP models can be easily interpreted using extreme upper quantiles or return levels. In hydrology, the return level is generally defined on an annual scale, e.g., for a return period N, N-year return level is defined as the level expected to be exceeded once in every N years, or having an exceedance probability of $1/N$ in any given year. N-year return level can be obtained by inverting equation (1) as

$$F^{-1}_{\sigma,\xi} = RL_N = \begin{cases} u + \frac{\sigma}{\xi}\left[\left(Nn_y\zeta_u\right)^{\xi} - 1\right], & \xi \neq 0 \\ u + \sigma\log\left(Nn_y\zeta_u\right), & \xi = 0, \end{cases}$$

where u and n_y are the threshold and number of observations in a year, respectively; and $\zeta_u = k/n$ is the probability of an individual observation exceeding u [*Coles*, 2001].

[9] The GP distribution is a limiting distribution of excesses over a large threshold, therefore the choice of threshold can be critical. If a threshold is low, it is likely to violate the asymptotic basis of the model leading to bias in estimation and extrapolation whereas a high threshold will result in small number of exceedances for model estimation leading to large estimation variance [*Coles*, 2001]. Two methods for threshold selection, which provide a reasonable approximation to the distribution of threshold excesses, are

available: (a) find a threshold u_0 from the mean residual plot, which is a plot between mean of excesses and threshold u, above which the plot is approximately linear in u, and (b) find a threshold u_0 above which the estimates of ξ and σ are constant [*Coles*, 2001]. These threshold choices are based on user judgments or subjective considerations. This study does not use any of the above methods for threshold selection because it is not feasible to select thresholds based on visual inspection at each and every grid point from 223 grid points in South America. Since the extreme precipitation events are assumed to be rare, the selection of a constant threshold for all spatial grid points is not recommended because this may give more number of extremes at some places or less/no extremes at other places. A spatially distributed threshold is more justifiable hydrologically because the impact of large precipitation is likely to depend on deviation from the *usual* at any given spatial location. Previous researchers chose some high quantiles, e.g., 97.5% and 95%, of the empirical distributions as thresholds [*Easterling et al.*, 2000; *Meehl and Tebaldi*, 2004]. In this study, we choose thresholds as the 99%-quantile and 95%-quantile of the daily and weekly maxima data, respectively.

2.2.2. Precipitation Extremes Volatility Index (PEVI)

[10] Hydraulic structures or other civilian infrastructures are often designed to withstand extremes events of certain magnitudes. However, the infrastructures may fail if they are exposed to a rarer and more intense extreme event. A measure that compares the increase in intensity with the rarity of extreme events can be a useful indicator for vulnerability, assuming all other conditions remain the same. Assuming $T > t$, if the T-year event, which corresponds to a $(1/T)$ probability of occurrence, were to be marginally higher than the t-year design event with a $(1/t)$ probability, the infrastructures can be considered to be less vulnerable compared to a situation where the difference between the intensities is significant. The difference in the intensities correspond to a measure of surprise when a lower probability and more intense extreme event occurs compared to the design event. The PEVI is a new measure defined in this study to quantify and visualize the anticipated surprise caused by intense extreme precipitation events. This measure is calculated here as a ratio of return levels, i.e., RL_T/RL_t, where $T > t$; RL_T and RL_t are T-year and t-year RLs, respectively. The PEVI does not contain any new information from the point of view of extreme value theory since the information contained in it can also be derived from ξ and RLs obtained from the GP distribution. The PEVI is theoretically satisfying since there is a direct relation with ξ given as

$$PEVI = \frac{RL_T}{RL_t} \sim \begin{cases} (T/t)^{\xi}, & \xi > 0, \\ \log(T)/\log(t), & \xi = 0, \\ 1, & \xi < 0. \end{cases}$$

The PEVI takes values greater or equal to one. The engineering intuition for RL_t is that it is a *design RL* for t years corresponding to which hydraulic structures have been designed or disaster readiness or mitigation systems have been put in place. RL_T is analogous to a higher bound on the *anticipated RL* for T years which has lower probability than RL_t but may nevertheless occur in any given year. If the PEVI is unity, the higher bound on the *anticipated RL* exactly equals the *design RL* implying very less probability of more intense extremes. However, the degree of surprise, when more intense extreme occurs, increases with larger values of PEVI. In this sense, the PEVI can also be used as the safety factor for engineering design. This study chooses T and t as 200 and 50 a, respectively. We also present the PEVI since it is statistically valid and can be computed relatively efficiently for each grid point. It can be more easily interpreted and visualized than the GP distribution parameters, which do not have an event-based intuitive interpretation. This provides a measure accessible not only to statisticians but also to hydrologists, climatologists, and decision-makers. The fact that the PEVI can be easily calculated and captured through a single number makes the application to high-resolution data over large geographical areas possible.

2.2.3. Quality of the Poisson-GP Model

[11] We investigate the quality of the Poisson process by comparing the distribution of inter-arrival times of threshold exceedances with the exponential distribution. The quality of the GP distribution to threshold excesses is investigated by examining probability and quantile plots obtained by fitting the GP distribution to threshold excesses.

[12] We compare the distribution of the inter-arrival times of threshold exceedances with the exponential distribution using the goodness-of-fit statistic D_{SP}, suggested by *Michael* [1983], which is based on the *stabilized probability plot*. Let $t_1,\ldots,t_k$ be k inter-arrival times of exceedances over threshold given as the 95%-quantile. If $t_1 < \ldots < t_k$ is an ordered sample drawn from an exponential distribution, whose cumulative distribution function is given as $F_0(t,\ \lambda) = 1 - e^{-\lambda t}$ for $t \geq 0$, the stabilized plot consists of coordinates, $(r_i,\ s_i)$, which can be calculated as

$$r_i = \frac{2}{\pi} \arcsin \sqrt{\frac{1}{k}\left(i - \frac{1}{2}\right)},$$
$$s_i = \frac{2}{\pi} \arcsin \sqrt{\frac{1}{\hat{\lambda}} F_0\left(t_i, \hat{\lambda}\right)},$$

where $\hat{\lambda}$ is the maximum likelihood estimator of λ under an exponential distribution. From the stabilized plot, the deviations of plotted points from a line joining (0, 0) and (1, 1) indicate departures from their theoretical values [*Coles*, 1989]. One attractive property of the stabilized plot is that the variances of plotted points are approximately equal [*Michael*, 1983]. This property motivates the definition of a goodness-of-fit statistic D_{SP} given as

$$D_{\mathrm{SP}} = \max_{i=1,\ldots,k} |r_i - s_i|,$$

which measures the maximum deviation of the plotted points from their theoretical values and removes the subjectivity in the interpretation of stabilized plots [*Michael*, 1983]. D_{SP} is analogous to and more powerful than the standard Kolmogorov-Smirnov statistic [*Michael*, 1983; *Kimber*, 1985]. D_{SP} is used here to measure the maximum deviation of the inter-arrival times of threshold exceedances from an exponential distribution. In order to test goodness-of-fit of the inter-arrival times to the exponential distribution, D_{SP} can be compared with critical values D^*_{SP}. D^*_{SP}

is obtained as some sample quantile recorded from m number of samples of sample size n [*Coles*, 1989]. *Coles* [1989] calculated D^*_{SP} as 95%-quantile of 10000 samples of size 10, 25, and 40 data points for normal, logistic, Cauchy, and double exponential distributions. Since this study analyzes 223 grid points and each grid point can have 728 to 3380 data points, i.e., 14 to 65 a of weekly data, in the interests of computational tractability, we consider 1000 samples for the calculation of D^*_{SP}. We generate 1000 independent samples of sample size n and calculate $D^{\text{sim } m}_{SP}$ from the inter-arrival times of exceedances over the threshold of 95%-quantile of mth sample for each m = 1,...,1000. We choose D^*_{SP} as the 95%-quantile of $D^{\text{sim } m}_{SP}$, m = 1,...,1000. If $D_{SP} \leq D^*_{SP}$, we do not reject the assumption that the inter-arrival times of threshold exceedances are independent and exponentially distributed. In order to compare D_{SP} and D^*_{SP}, we define a simple measure as

$$\overline{D}_{SP} = \frac{D_{SP}}{D^*_{SP}}.$$

If $\overline{D}_{SP} > 1$, we reject with 95% confidence that the inter-arrival times of threshold exceedances are exponentially distributed, hence the inter-arrival times of threshold exceedances do not follow one-dimensional *homogeneous Poisson process*. If $\overline{D}_{SP} \leq 1$, we do not reject the assumption that the inter-arrival times of threshold exceedances follow one-dimensional *homogeneous Poisson process*. This study uses $\overline{D}_{SP}$ at all 223 grid points because it can be easily computed, plotted and visualized in space for comparisons.

[13] The quality of the fitted GP model to threshold excesses can be checked using probability and quantile plots. If $y_1, \ldots, y_k$ are the k excesses over a threshold u and $\hat{F}$ is an estimated GP model, the probability plot can be generated as

$$\left\{\left(i/(k+1), \hat{F}(y_i)\right); i = 1, \ldots, k\right\},$$

where

$$\hat{F}(y) = \begin{cases} 1 - \left[1 + \left(\hat{\xi}y/\hat{\sigma}\right)\right]^{-1/\hat{\xi}}, & 1 + \left(\hat{\xi}y/\hat{\sigma}\right) > 0, \ \hat{\xi} \neq 0 \\ 1 - e^{-y/\hat{\sigma}}, & \hat{\xi} = 0, \end{cases}$$

where $\hat{\sigma}$ and $\hat{\xi}$ are the estimated values of σ and ξ, respectively. The quantile plots can be generated by plotting the points as

$$\left\{\left(\hat{F}^{-1}(i/(k+1)), y_i\right); i = 1, \ldots, k\right\},$$

where

$$\hat{F}^{-1}(y) = u + \frac{\hat{\sigma}}{\hat{\xi}}\left[y^{-\hat{\xi}} - 1\right].$$

Both probability and quantile plots should consist of points lying close to the unit diagonal if the GP model is appropriate for modeling threshold excesses [*Coles*, 2001]. Goodness of fit tests for the GP distributions, e.g., Anderson-Darling or Cramer-von Mises, as well as independence tests, e.g., Kendall's τ, exist and may need to be explored in more detail in future follow-on studies.

2.3. Data Preparation for the Validity of the Poisson-GP Model

[14] The validity of the Poisson-GP model is based on the assumption that the data should be IID. The presence of long term trends, seasonality, and temporal correlations violate the assumption of IID data [*Gaines and Denny*, 1993]. Precipitation data may be temporally correlated and have long term or seasonal trends [*Gaines and Denny*, 1993]. *Galambos* [1987] investigated the effect of long term trends, seasonality, and temporal dependence in the data on the validation of extreme value theory and found that if the auto-correlation decreases as lag times increases, the asymptotic distribution of extremes is the same as that from IID samples. The detection of clustering of extremes is also important because maximum likelihood estimation technique assumes the time series of excesses over a large threshold to be independent [*Katz et al.*, 2005]. Clustering gradually disappears as the threshold increases but there are some variables, such as temperature, which exhibit clustering even with high thresholds [*Coles*, 2001]. If there exists clusters of extremes over a high threshold, *Todorovic and Zelenhasic* [1970] presented an ad hoc and inefficient procedure for declustering which generates a time series by choosing the highest value of each cluster.

[15] We analyze three different sets of data generated from the daily data, such as daily, weekly maxima, and weekly maxima residuals, to choose the best data satisfying the IID assumption and improving the quality of the Poisson-GP model. Instead of presenting the results from 223 grid points, we outline the results for two grid points representing two very different scenarios. Each of these two grid points has 65 a of daily precipitation and their locations are given in terms of (*longitude*, *latitude*) as (315, −10) and (310, −25). At these two grid points, we examine time series plots for detecting seasonal trends and auto-correlation plots for detecting temporal dependence. We detect the clustering of extremes by plotting threshold excesses at these grid points. We also compare $\overline{D}_{SP}$ for the quality of the Poisson process, probability and quantile plots for the quality of the GP distribution from daily, weekly maxima, and weekly maxima residuals in our quest to find the best data for the analysis. For $\overline{D}_{SP}$, we analyze daily, weekly maxima, and weekly maxima residuals data for all 223 grid points in South America for three time windows, i.e., 1940–2004, 1965–1989, and 1980–2004.

2.3.1. Daily

[16] We first analyze daily precipitation data to check if the IID assumption for the Poisson-GP model is satisfied. The threshold is chosen as the 99%-quantile of time series at each grid point. For 1940–2004, the time series, excesses over the threshold, and auto-correlation plots for two grid points, i.e., (315, −10) and (310, −25), are shown in Figures 2 and 3, respectively. We do not observe any long term trends at both grid points but they do show the presence of seasonality and temporal dependence. The grid point (315, −10) shows greater seasonality and temporal dependence as compared to (310, −25). A total of 88%, 85%, and 82% grid points show significant auto-correlations by visual inspection for the period 1940–2004, 1965–1989,

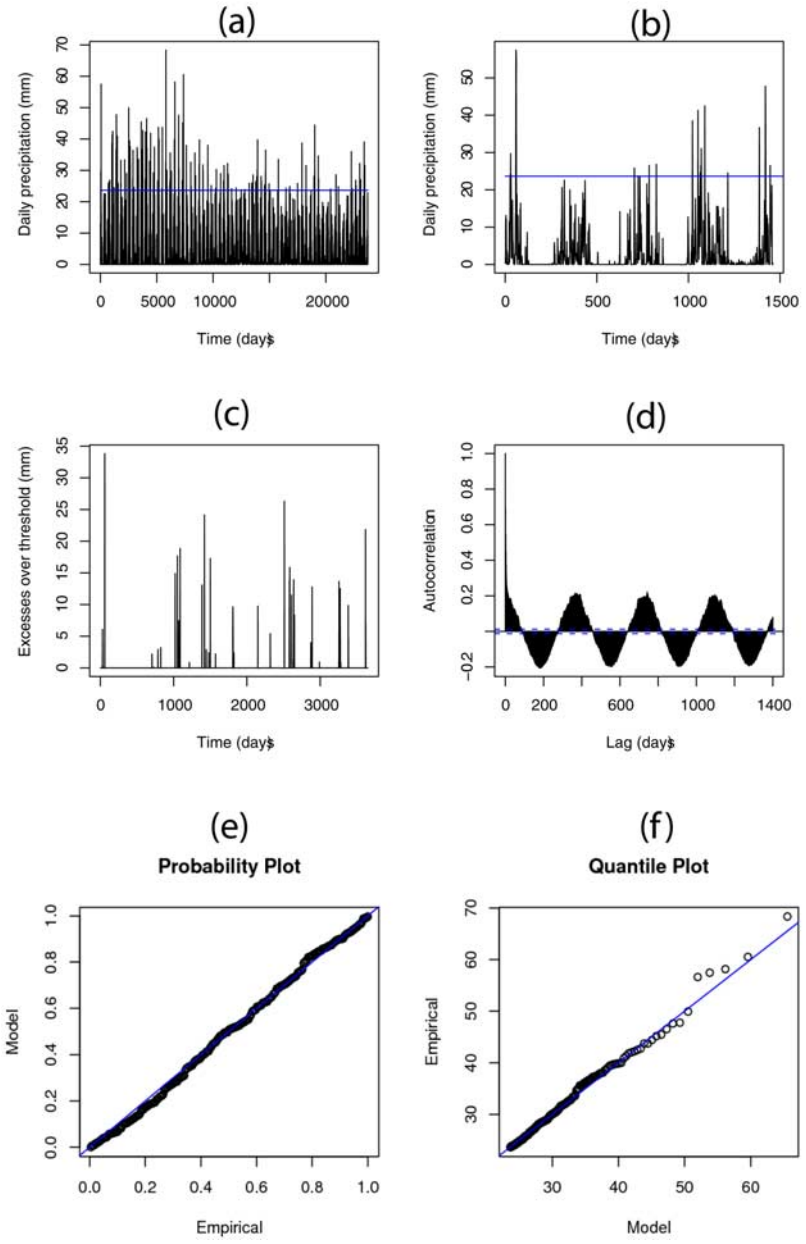

Figure 2. Grid point having (*longitude*, *latitude*) as (315, −10): Daily data with threshold given as 99%-quantile (shown as a horizontal line in blue in (a) and (b)). (a) Time series for 65 a; (b) Time series for 4 a; (c) Excesses over a threshold for the first 10 a; (d) Auto-correlation plot; (e) Probability plot; and (f) Quantile plot. We observe strong seasonality and temporal dependence and also some clustering of extremes. The quality of probability and quantile plots is poor.

and 1980–2004, respectively. We do observe some clusters at both grid points (Figures 2a, 2c, 3a, and 3c) but do not use here the declustering method suggested by *Todorovic and Zelenhasic* [1970] since the definition of clusters is based on subjective considerations which makes this declustering procedure inefficient for 223 grid points. $\overline{D}_{SP}$ is more than one at a majority of locations in South America which means that we reject with 95% confidence that the interarrival times of threshold exceedances follow a *homogeneous Poisson process* at these locations (Figure 4a). The quality of probability and quantile plots obtained by fitting the GP distribution to daily data is good at (310, −25) but poor at (315, −10) (Figures 2e, 2f, 3e, and 3f). On the basis of all the above reasons, this study rules out the analysis of daily precipitation for the investigation of spatial and temporal variability of extremes using the Poisson-GP model. Therefore we aggregate daily data into weekly maxima data in order to check if it reduces temporal dependence, resolves the clustering problem and improves $\overline{D}_{SP}$ (described in the next section).

2.3.2. Weekly Maxima

[17] We generate weekly maxima precipitation time series from daily precipitation at each grid point. In this case, the threshold is chosen as the 95%-quantile of time series at

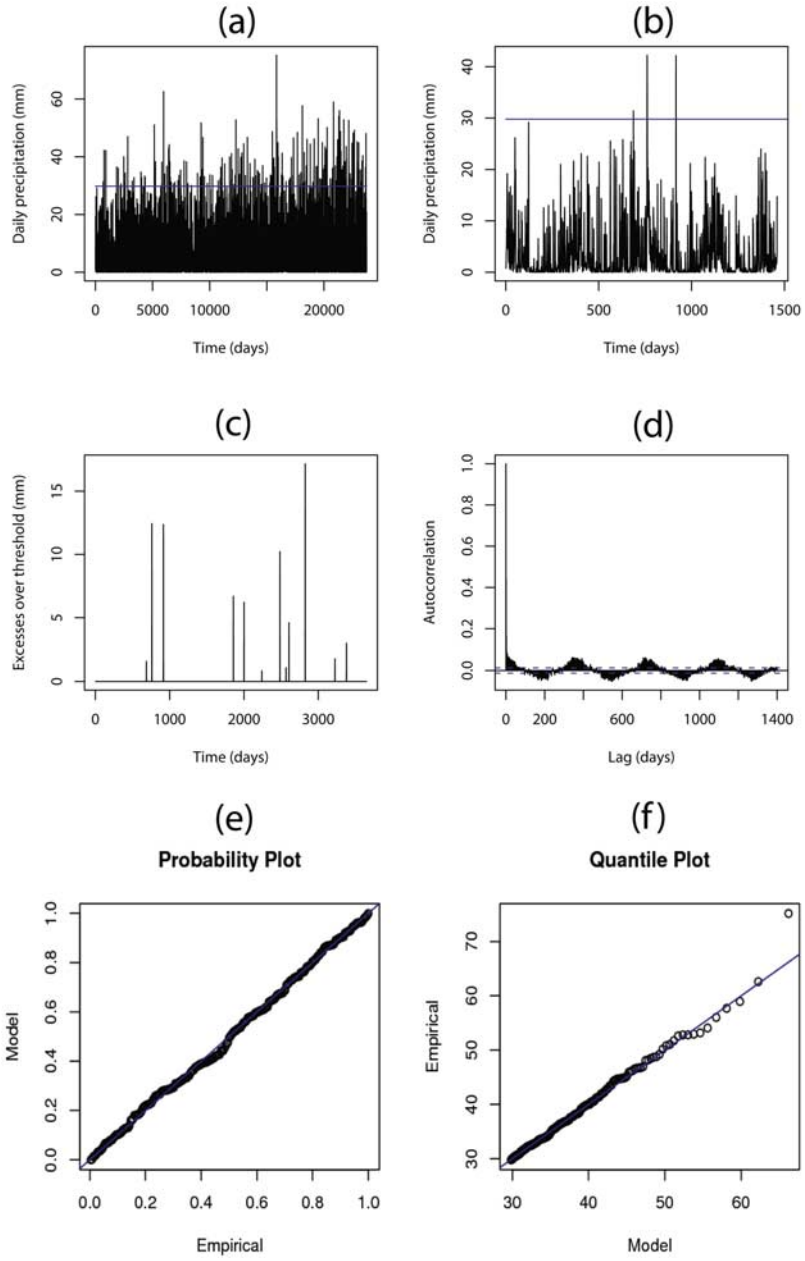

Figure 3. Grid point having (*longitude*, *latitude*) as (310, −25): Daily data with threshold given as 99%-quantile (shown as a horizontal line in blue in (a) and (b)). (a) Time series for 65 a; (b) Time series for 4 a; (c) Excesses over a threshold for the first 10 a; (d) Auto-correlation plot; (e) Probability plot; and (f) Quantile plot. The seasonal patterns are weak but there exists temporal dependence and clusters of extremes. The quality of probability and quantile plots is good.

each grid point. Both grid points, i.e., (315, −10) and (310, −25), do not show any long term trends (Figures 5a and 6a). At (315, −10), we do not observe significant changes in seasonality and clustering of extremes from weekly maxima as compared to daily data but weekly maxima shows greater temporal dependence than daily as shown by auto-correlation plots (Figures 2b, 2c, 2d, 5b, 5c, and 5d). At (310, −25), significant improvements are observed in seasonality, clustering of extremes, and temporal dependence from weekly maxima if compared with daily (Figures 3b, 3c, 3d, 6b, 6c, and 6d). We do observe some temporal dependence in weekly maxima data at (310, −25) (Figure 6d). Visual inspection of auto-correlation plots for all grid points indicates significant auto-correlations in nearly 80%, 80%, and 77% grid points for the period 1940–2004, 1965–1989, and 1980–2004, respectively. At both grid points, the quality of probability and quantile plots from weekly maxima degrades if compared with daily (Figures 2e, 2f, 3e, 3f, 5e, 5f, 6e, and 6f). $\overline{D}_{SP}$ shows slight improvements as compared to that from daily but it is more than one at the majority of grid points in South America (Figure 4b).

[18] The results discussed and presented in this section provide a couple of interesting insights, which, in turn, have influenced our data analysis choices. First, minor to rela-

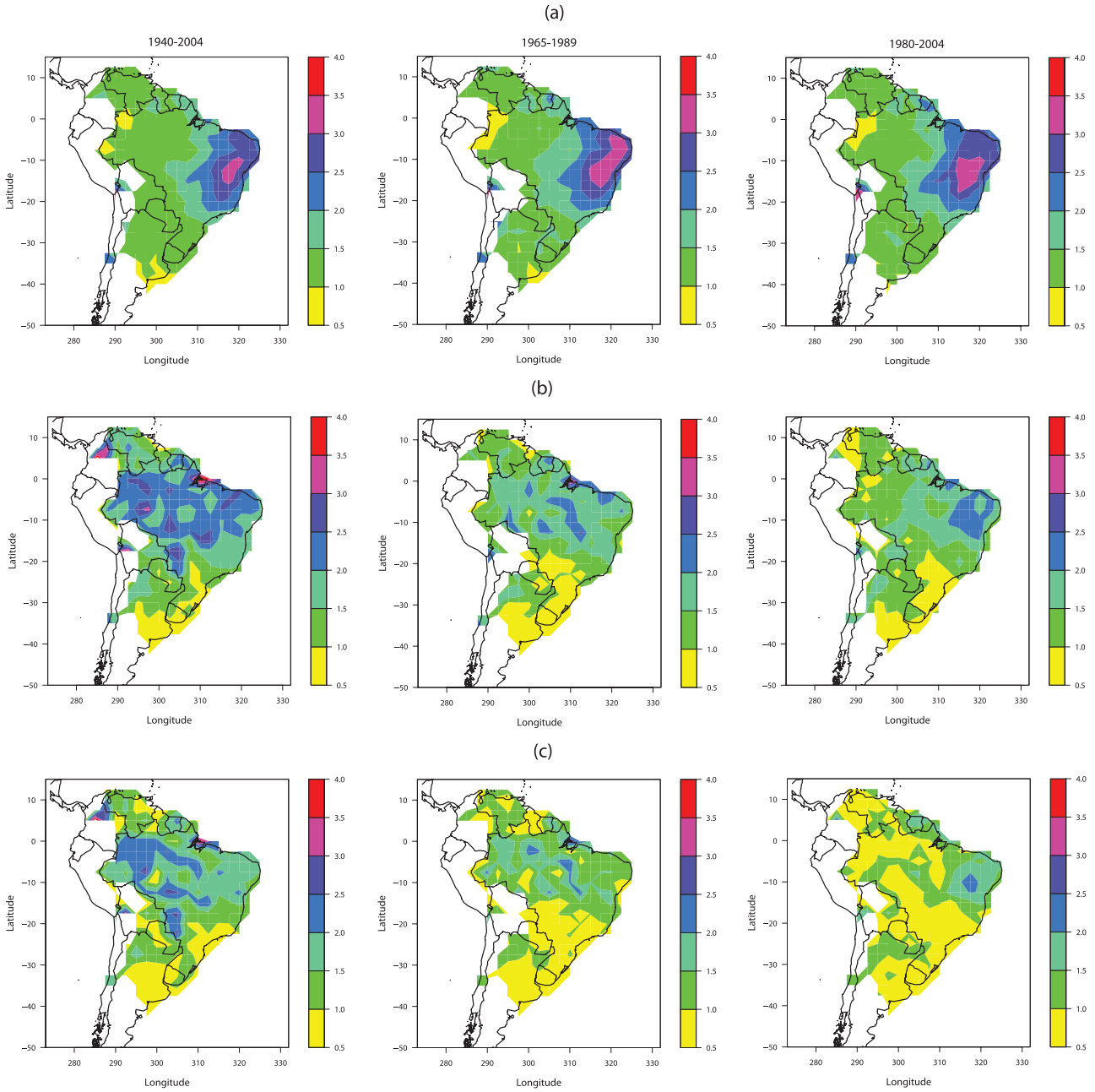

Figure 4. $\overline{D}_{SP}$ for three time windows, i.e., 1940–2004, 1965–1989, and 1980–2004: (a) daily data; (b) weekly maxima; and (c) weekly maxima residuals. If $\overline{D}_{SP} \leq 1$, we do not reject the assumption that the inter-arrival times of threshold exceedances follow one-dimensional *homogeneous Poisson process*. There is significant improvement in $\overline{D}_{SP}$ from weekly maxima residuals over daily and weekly maxima data for all three time windows.

tively more significant reductions, in terms seasonality or periodicity, clustering of extremes and autocorrelation, as well as improvements in terms of the $\overline{D}_{SP}$ measure, are observed from the analysis of weekly maxima data compared to the corresponding daily data. This leads us to choose weekly data in this study as they appear better suited to the type of extreme value analysis utilized here. The fact that daily precipitation data exhibit correlations with nearby lags in well-known and has been used, for example, in weather simulations [*Rajagopalan and Lall*, 1999]. On the other hand, the correlations are known to decay quickly and expected to be less significant at weekly timescales. While a combination of our data analysis results with known statistical insights about precipitation leads us to the choice of weekly data, we believe that analysis of daily data, potentially after creative post-processing designed to reduce the observed dependence, may yield interesting insights. However, the success of the post-processing scheme may determine our degree of belief in the results of the extreme value theory and therefore the scheme may need to get into rather involved modeling of precipitation processes. This is left as an area of future research. The second insight is that even

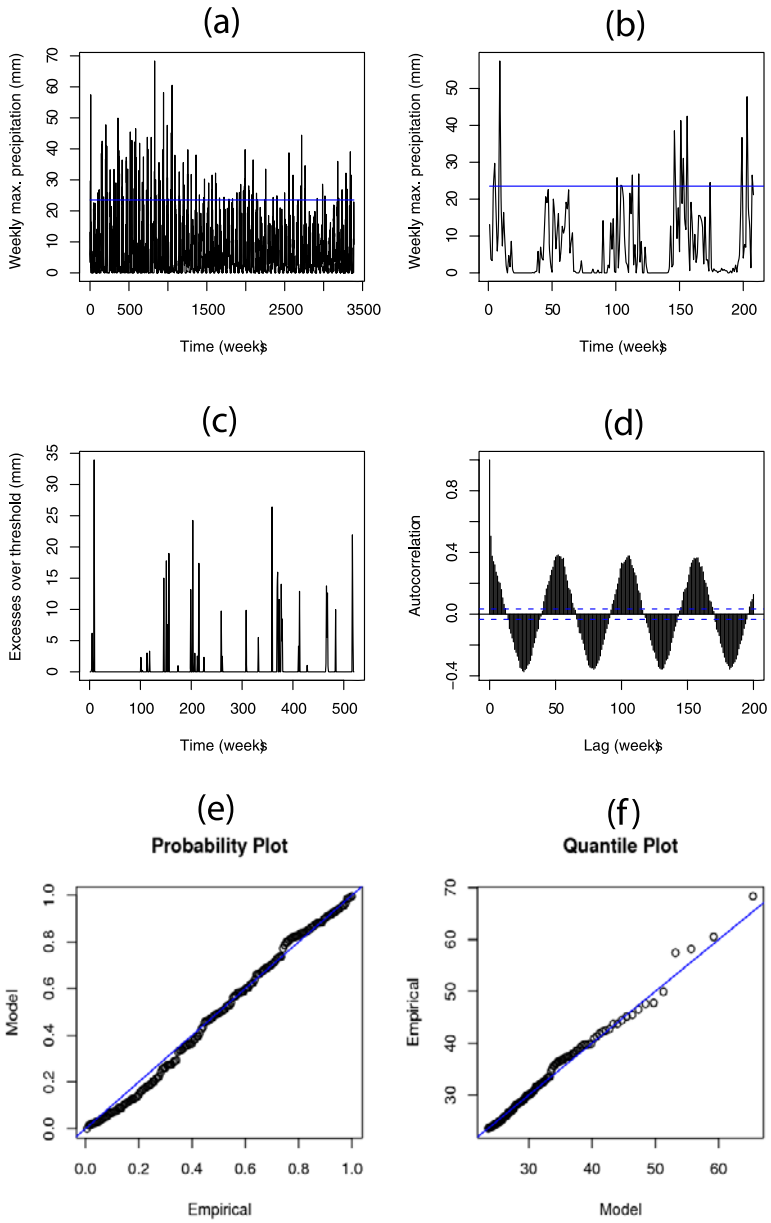

Figure 5. Grid point having (*longitude*, *latitude*) as (315, −10): Weekly maxima data with threshold given as 95%-quantile (shown as a horizontal line in blue in (a) and (b)). (a) Time series for 65 a; (b) Time series for 4 a; (c) Excesses over a threshold for the first 10 a; (d) Auto-correlation plot; (e) Probability plot; and (f) Quantile plot. We observe strong seasonal patterns, clusters of extremes, and temporal dependence. The quality of probability and quantile plots is bad.

the weekly aggregated data, while apparently more suitable than daily data, continues to retain seasonal or periodic patterns and short-term temporal dependence. This leads us to further investigate whether such patterns and dependence can be reduced from weekly data prior to extreme value analysis (described in the next section).

2.3.3. Weekly Maxima Residuals

[19] We use a brute-force approach described by *Gaines and Denny* [1993] to remove seasonality from weekly maxima to generate weekly maxima residuals. Weekly maxima residuals are obtained by subtracting the long term mean of weekly maxima of a particular week, i.e., mean of maximum weekly precipitation across the same week for all years used in the analysis, from weekly maxima of the same week. At each grid point, the threshold is chosen as the 95%-quantile of time series. Long term trends at both grid points, i.e., (315, −10) and (310, −25), are absent (Figures 7a and 8a). At (315, −10), seasonality and temporal dependence are still present for weekly maxima residuals data but it has the lowest temporal dependence as compared to daily and weekly maxima data sets (Figures 2b, 2d, 5b, 5d, 7b, and 7d). At (310, −25), clustering of extremes from weekly maxima residuals is not different from weekly maxima (Figures 6c and 8c). There is no seasonality and temporal dependence in weekly maxima residuals at (310, −25) (Figures 8b and 8d). For weekly maxima residuals, nearly

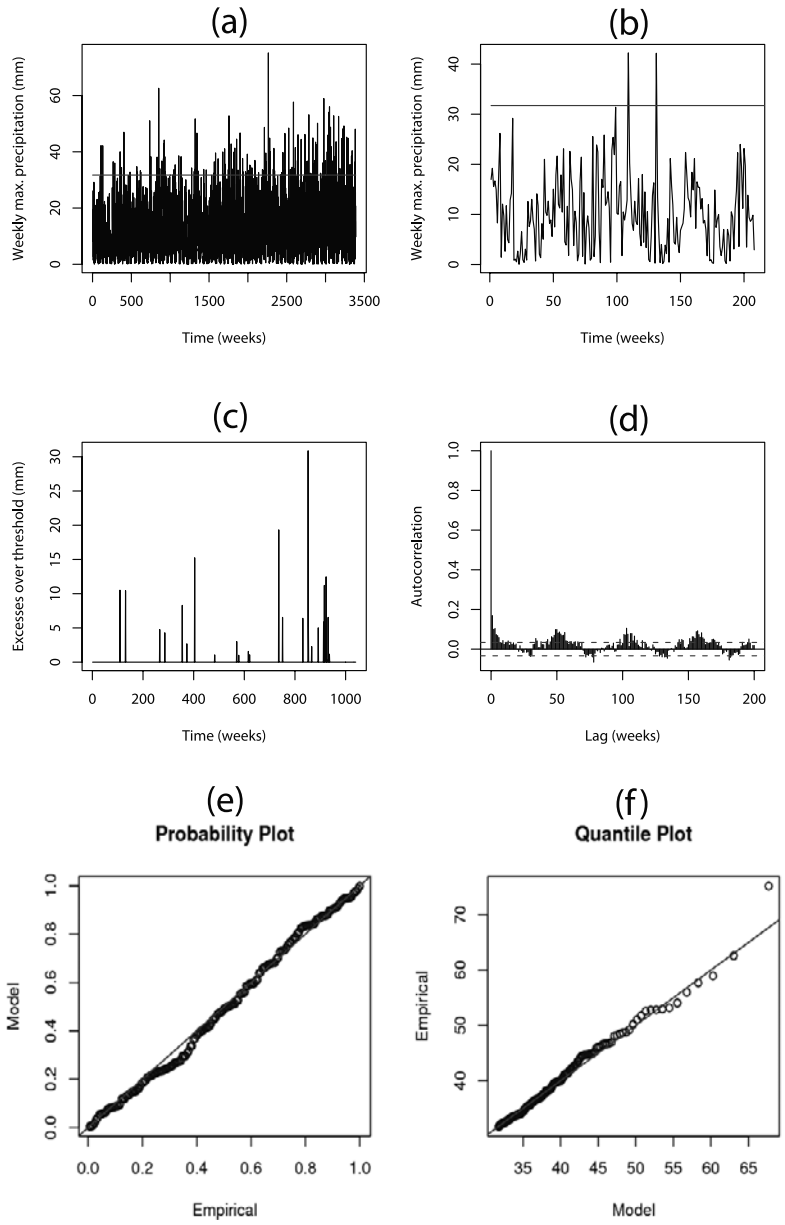

Figure 6. Grid point having (*longitude*, *latitude*) as (310, −25): Weekly maxima data with threshold given as 95%-quantile (shown as a horizontal line in blue in (a) and (b)). (a) Time series for 65 a; (b) Time series for 4 a; (c) Excesses over a threshold for the first 20 a; (d) Auto-correlation plot; (e) Probability plot; and (f) Quantile plot. The seasonal patterns are not evident from time series plots and there is some improvement in clustering of extremes as compared to daily data (Figure 3c). We observe some temporal dependence but it seems to be of the same order as from daily (Figure 3d). The quality of probability and quantile plots is good but not better than the plots from daily (Figures 3e and 3f).

58%, 56%, and 46% grid points show significant temporal dependence by visual inspection of auto-correlation plots for the period 1940–2004, 1965–1989, and 1980–2004, respectively, which indicates significant improvement if compared with the respective figures from daily or weekly maxima. At both grid points, probability and quantile plots consist of points lying closer to the unit diagonal indicating that the GP distribution is reasonable for modeling threshold excesses (Figures 7e, 7f, 8e, and 8f). $\overline{D}_{\mathrm{SP}}$ for 1940–2004, 1965–1989, and 1980–2004 show significant improvements over daily and weekly maxima data since $\overline{D}_{\mathrm{SP}} \leq 1$ or $\overline{D}_{\mathrm{SP}}$ lies between 1 and 1.5 at the majority of places in South America for all time periods (Figure 4c). For 1965–1989 and 1980–2004, $\overline{D}_{\mathrm{SP}}$ from weekly maxima residuals is less than one in more than 50% of total grid points considered in this study (Figure 4c). As we move from daily to weekly maxima residuals data for 1940–2004, $\overline{D}_{\mathrm{SP}}$ changes from greater than two to less than two for grid (315, −10) whereas it changes from greater than one to less than one for (310, −25) (Figures 4a and 4c). It is interesting to note that the temporal dependence go away completely if we consider weekly maxima residuals at (310, −25) where

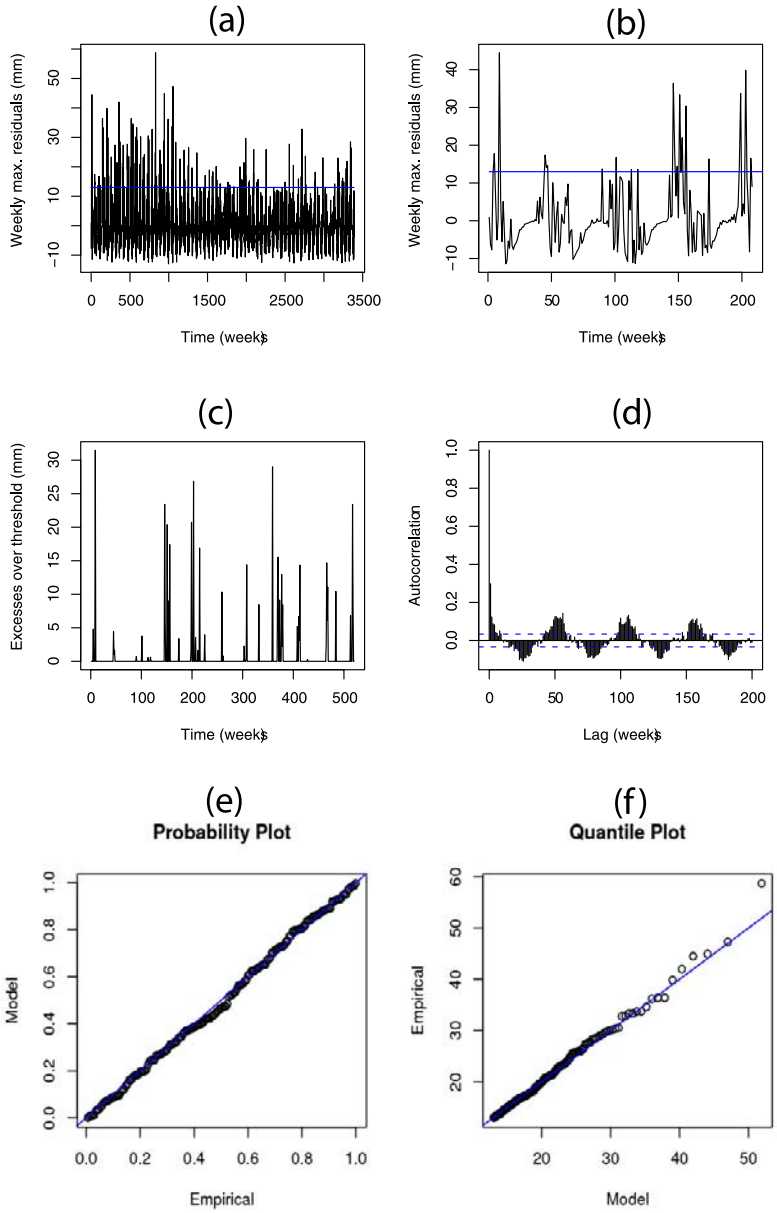

Figure 7. Grid point having (*longitude*, *latitude*) as (315, −10): Weekly maxima residuals data with threshold given as 95%-quantile (shown as a horizontal line in blue in (a) and (b)). (a) Time series for 65 a; (b) Time series for 4 a; (c) Excesses over a threshold for the first 10 a; (d) Auto-correlation plot; (e) Probability plot; and (f) Quantile plot. There exists strong seasonal patterns and clusters of extremes. We observe temporal dependence but it is less as compared to daily and weekly maxima (Figures 2d and 5d). The quality of probability and quantile plots is good and also better than that from daily and weekly maxima (Figures 2e, 2f, 5e, and 5f).

$\overline{D}_{SP}$ is less than one (Figures 4c and 8d). While temporal dependence persists even after considering weekly maxima residuals at (315, −10) where $\overline{D}_{SP}$ is between 1.5 and 2 (Figures 4c and 7d).

[20] The complete removal of seasonality from weekly maxima data is not possible by removing long term mean of weekly maxima from weekly maxima (Figure 7d). This process changes the order of magnitude of weekly maxima precipitation which leads to the changes in the order of magnitude of excesses over a threshold. However, both weekly maxima and weekly maxima residuals may produce most of the extremes based on their respective 95%-quantile thresholds at the same time but the excesses over their respective thresholds do not have the same magnitudes (Figures 5c, 7c, 6c, and 8c). This may happen because the selection of extremes is based on 95%-quantile threshold of each time series rather than based on a fixed threshold. We fit the GP distribution to excesses over 95%-quantile threshold (Figure 9) for both weekly maxima and weekly maxima residuals and plot the spatial variability of σ and ξ and their standard errors (Figures 10, 11a, 11b, 12a, and 12b). We observe that the spatial variability of σ and ξ from

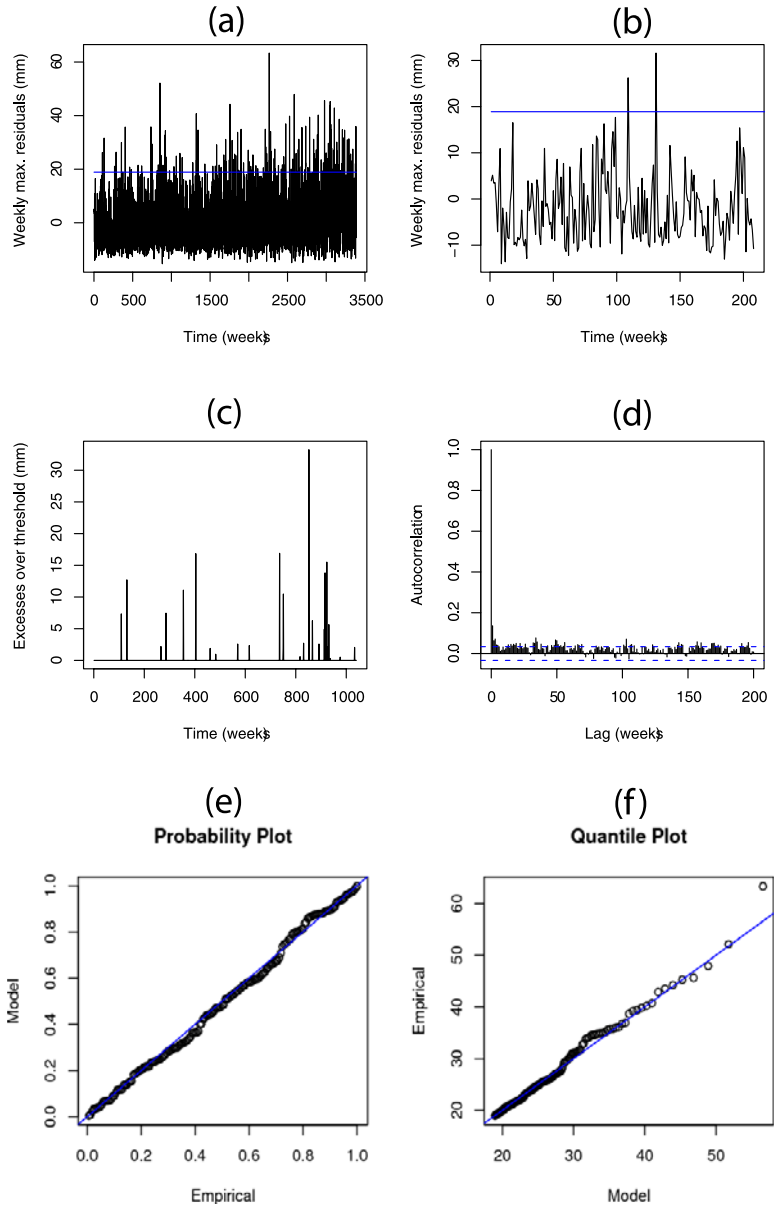

Figure 8. Grid point having (*longitude*, *latitude*) as (310, −25): Weekly maxima residuals data with threshold given as 95%-quantile (shown as a horizontal line in blue in (a) and (b)). (a) Time series for 65 a; (b) Time series for 4 a; (c) Excesses over a threshold for the first 20 a; (d) Auto-correlation plot; (e) Probability plot; and (f) Quantile plot. The seasonal patterns are absent. There is no improvement in clustering of extremes as compared to weekly maxima (Figure 6c). The temporal dependence disappears completely. We observe significant improvements in temporal dependence as compared to daily and weekly maxima (Figures 3d and 6d). The quality of probability and quantile plots is good.

weekly maxima residuals shows the same patterns as obtained from weekly maxima in the most parts of South America. However, we observe significant improvements in the standard errors of σ and ξ from weekly maxima residuals as compared to that obtained from weekly maxima. The probability and quantile plots at two grids, i.e., (315, −10) and (310, −25), indicate better quality of the fitted GP distribution from weekly maxima residuals as compared to that from weekly maxima (Figures 5e, 5f, 6e, 6f, 7e, 7f, 8e, and 8f). Since this study deals with the spatial and temporal variability of extremes, we may get the same spatial and temporal patterns from both weekly maxima residuals and weekly maxima and thus, may not affect our interpretation of the results. However, the analysis of weekly maxima residuals has an edge over weekly maxima because of its lower standard errors and improvements in the quality of probability and quantile plots. Weekly maxima residuals also show improvements in terms of temporal dependence and $\overline{D}_{SP}$ if compared with weekly maxima. Thus we utilize weekly maxima precipitation residuals for the analysis. *Yates et al.* [2003] also considered weekly precipitation residuals to understand the spatial and temporal dependencies of the climate variables. The effect of the deseasonalization procedure on the validity of the extreme value

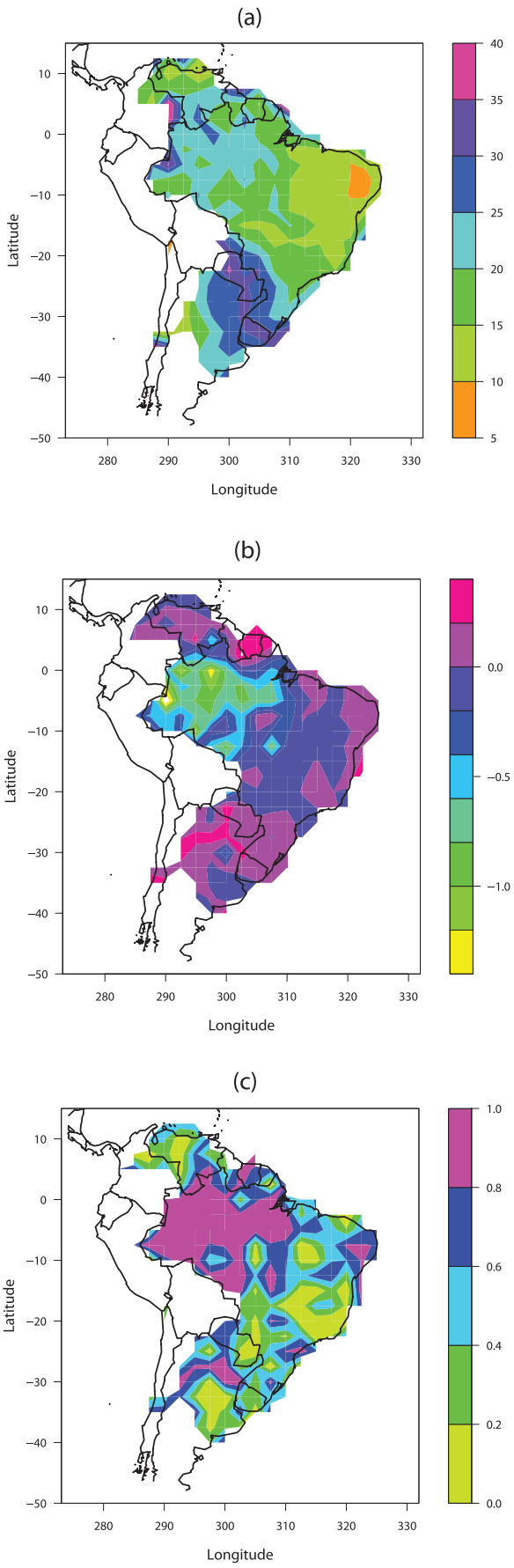

applications and parameter estimations may need to be investigated in more depth in subsequent research efforts.

3. Results and Discussions

[21] We analyze weekly maxima residuals to investigate the spatial and temporal variability of threshold, 50-a RL, 200-a RL, and PEVI (Figures 9, 13, 14, and 15). Increasing or decreasing trends in precipitation from 1965–2004 can be evaluated from the temporal variability of thresholds. At each grid point, the threshold is chosen as the 95%-quantile of time series. Spatial variability is investigated for 65 a (1940–2004) and the last 40 a (1965–2004) are analyzed for the temporal variability, which is given as the slope of linear trend obtained by fitting a regression line to 16 values computed from 25-a moving window from 1965–2004, i.e., 1965–1989, 1966–1990,. . ., 1980–2004. Using the GP distribution, the spatial and temporal variations in σ and ξ and their standard errors are evaluated and shown in Figures 11 and 12. σ ranges from 5–15 mm at major parts of South America except some parts of the Amazon basin, north Argentina, and Paraguay where it is more than 15 mm whereas the standard error of σ varies from 0-3 mm in the whole South America (Figures 11a and 11b). From 1965–2004, σ increases in eastern Brazil including Rio De Janeiro and major parts of the Brazilian Highlands, Uruguay, Paraguay, some parts of north Argentina, south Venezuela, French Guiana and Suriname whereas decreasing trends in σ are observed in the Amazon basin, Venezuela, the Mato Grasso Plateau, Catingas, São Paulo, and Buenos Aires (Figure 11c). ξ is mostly greater than zero in the whole South America except eastern Brazil and north Argentina (Figure 12a). ξ ranges from 0.4–0.6 and 0.2–0.4 in the Catingas and Mato Grasso Plateau, respectively. The standard error of ξ varies from 0.05–0.15 in the whole South America (Figure 12b). From 1965–2004, the temporal variations in ξ indicate increasing trends in Venezuela, eastern Brazil including Rio De Janeiro and São Paulo, and major parts of the Amazon basin, the Brazilian Highlands, Uruguay, Paraguay, and north Argentina including Buenos Aires (Figure 12c).

[22] The daily data is analyzed to investigate the spatial and temporal variability of consecutive 2- and 3-days extremes (Figure 16). In this case, the threshold is chosen as the 99%-quantile of daily time series. The consecutive 2- and 3-days are defined in terms of the percentage of the number of extremes occurring consecutively for 2- and 3-days out of the total number of extremes. We also investigate the spatial variations of monthly extremes which is defined as the percentage of the number of extremes

Figure 9. Threshold in mm, defined as the 95%-quantile of weekly maxima residuals at each grid point: (a) Spatial variability of threshold from 1940–2004; (b) Temporal variability at each point from 1965–2004 given as the slope of linear trend obtained by fitting a regression line to 16 threshold values computed from 25-a moving window from 1965–2004, i.e., 1965–1989, 1966–1990,. . ., 1980–2004; and (c) R^2 obtained from the regression line, which provides an overall measure of the quality of linear trends shown in (b). In (b), the white region at a location given by (*longitude*, *latitude*) as (290, −5) indicates −1.64.

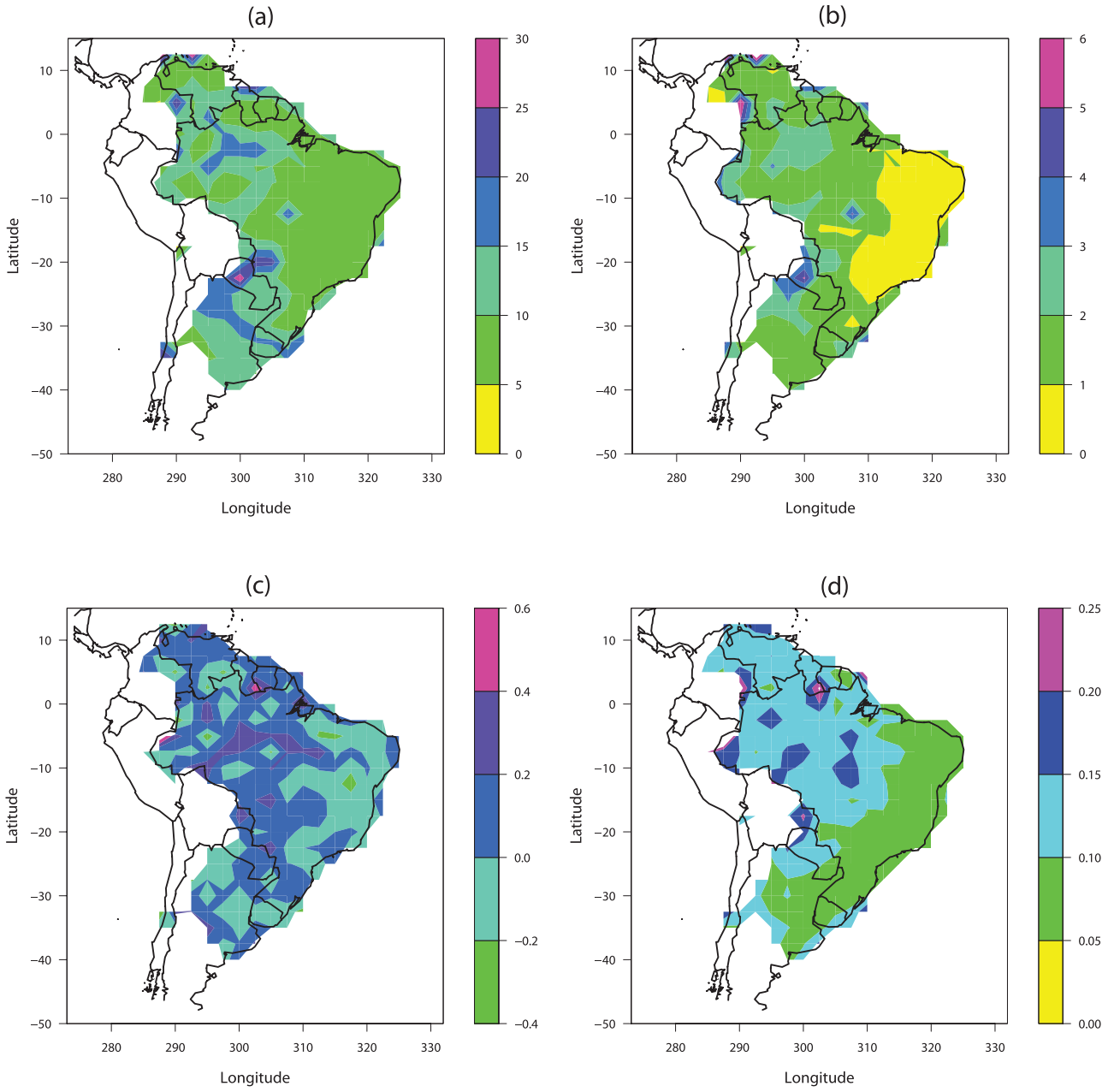

Figure 10. Scale (σ) and shape (ξ) parameters and their standard errors from weekly maxima precipitation for 1940–2004: (a) Spatial variability of σ in mm; (b) Spatial variability of standard errors of σ in mm; (c) Spatial variability of ξ; and (d) Spatial variability of standard errors of ξ.

occurring in a particular month out of the total number of extremes (Figure 17).

[23] Individual nations need to make policy decisions about water resources, agricultural planning, infrastructure management and disaster readiness or mitigation strategies. Thus we present our results by countries in 3.1–3.6. An investigation of precipitation extremes in conjunction with topography and vegetation, which is presented in 3.7, can lead to enhanced hydrological and climatological insights.

3.1. Brazil

[24] In the Amazon basin, threshold is larger than the other parts of Brazil but shows a decreasing trend from 1965–2004 (Figure 9). In the eastern parts of the Amazon basin, 50-a and 200-a RLs and their standard errors are higher than the other parts of South America but these RLs decrease more sharply as compared to the other parts of South America from 1965–2004 (Figures 13 and 14). Both 50-a and 200-a RLs show decreasing trends from 1965–2004 in the whole basin (Figure 14). The PEVI is higher in some eastern parts of the basin but it decreases sharply from 1965–2004 in those parts (Figure 15). We observe increasing PEVI trends from 1965–2004 in the major parts of the basin including north-west (NW) where it shows sharply increasing trends. The percentage of the number of consecutive 2-days extremes is less than 10% whereas the major parts of the basin have zero number of consecutive 3-days

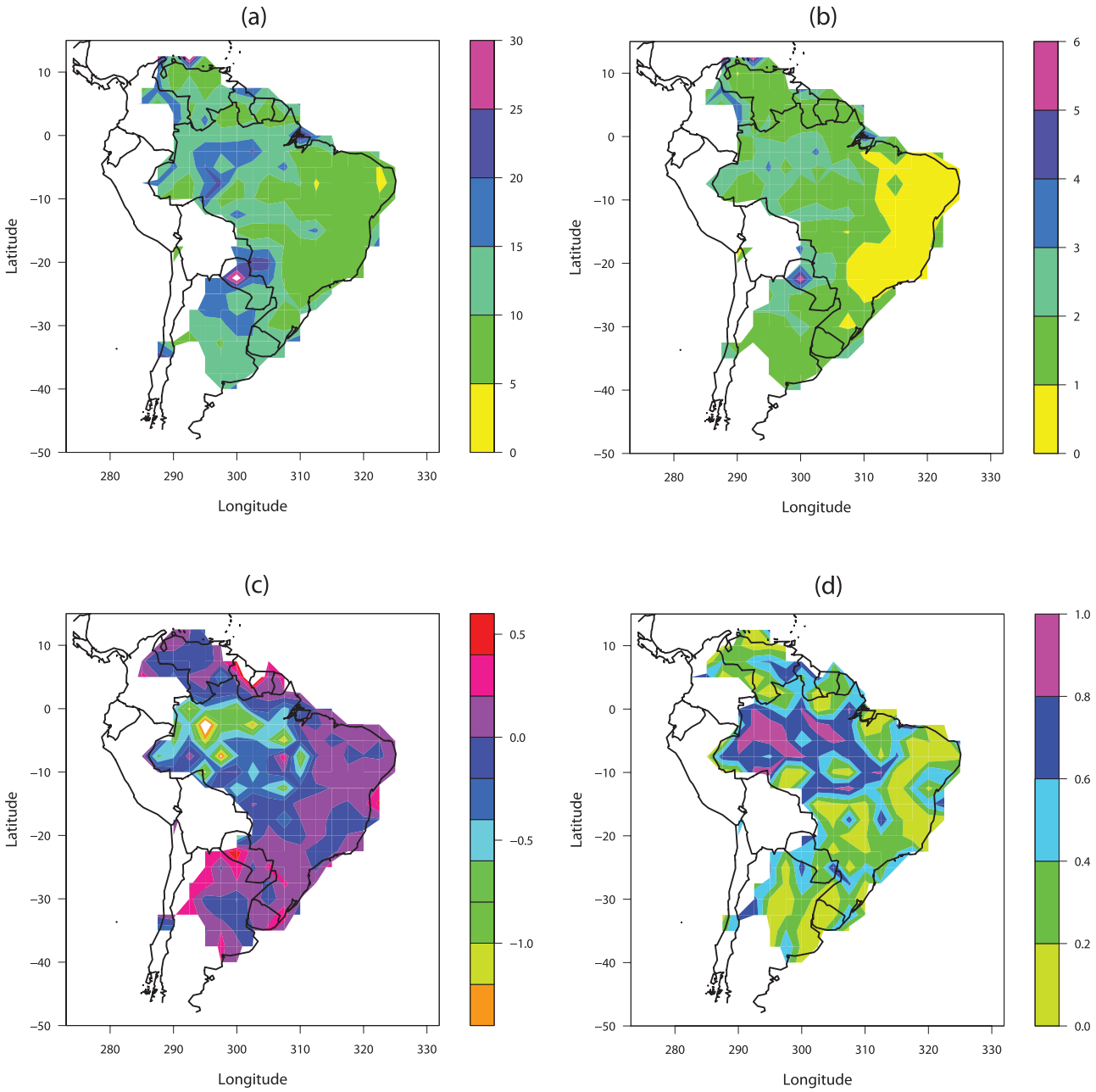

Figure 11. Scale parameter (σ) and its standard errors in mm from weekly maxima precipitation residuals: (a) Spatial variability of σ from 1940–2004; (b) Spatial variability of standard errors of σ from 1940–2004; (c) Temporal variability from 1965–2004; and (d) R^2 from linear trends shown in (c). In (c), the white region at a location given by (*longitude*, *latitude*) as (295, −2.5) indicates −1.77.

extremes (Figures 16a and 16b). From 1965–2004, the percentage of consecutive 2-days extremes increases only in the western parts of the basin whereas no trends in the percentage of consecutive 3-days extremes are observed because of zero number of consecutive 3-days extremes in the basin (Figures 16c and 16d).

[25] In Catingas and the Mato Grasso Plateau, thresholds are lower and show decreasing trends from 1965–2004 (Figure 9). Catingas has the highest 50-a RL, 200-a RL, and PEVI but their trends indicate downward behavior from 1965–2004 (Figures 13, 14, and 15). In the Mato Grasso Plateau, the PEVI is higher relative to the major parts of South America and lies between 1.4 and 1.5 but it shows a decreasing trend from 1965–2004 (Figure 15). The number of consecutive 2- and 3-days extremes are less than 10% and 2% of the total extremes, respectively, in both Catingas and the Mato Grasso Plateau (Figures 16a and 16b). From 1965–2004, the percentage of consecutive 2-days extremes shows increasing trends in Catingas and some parts of the Mato Grasso Plateau whereas the percentage of consecutive 3-days extremes indicates increasing and deceasing trends in Catingas and the Mato Grasso Plateau, respectively (Figures 16c and 16d).

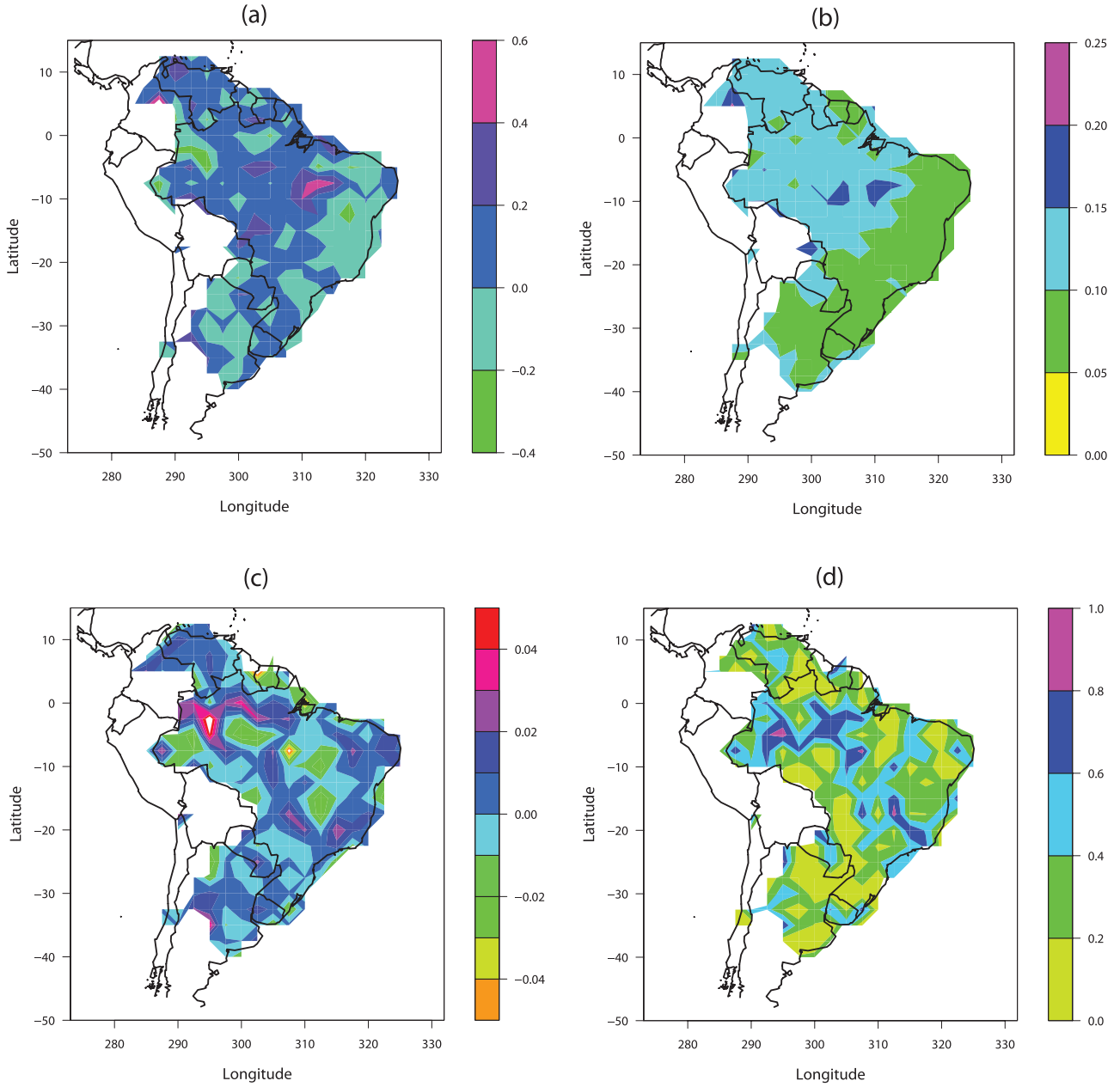

Figure 12. Shape parameter (ξ) and its standard errors from weekly maxima precipitation residuals: (a) Spatial variability of ξ from 1940–2004; (b) Spatial variability of standard errors of ξ from 1940–2004; (c) Temporal variability from 1965–2004; and (d) R^2 from linear trends shown in (c). In (c), the white region at a location given by (*longitude*, *latitude*) as (295, −2.5) indicates 0.063.

[26] In the Brazilian Highlands, threshold is low but it shows an increasing trend in the southern parts (Figure 9). Thresholds are low in east Brazil except south eastern Brazil where they are much higher relative to the other parts of South America. From 1965–2004, we observe increasing trends in threshold along eastern coastal regions of Brazil including Rio De Janeiro but thresholds show decreasing trends in Brasilia, São Paulo and their surrounding regions. 50-a RL, 200-a RL, and PEVI are low in the Brazilian Highlands and east Brazil but they show increasing trends in the major parts of the Brazilian Highlands and east Brazil including Rio De Janeiro and São Paulo (Figures 13, 14, and 15). In Brasilia, decreasing trends in PEVI are observed from 1965–2004 (Figure 15). 20-35% and 6-16% of the total extremes occur consecutively for 2 and 3 days, respectively, in the Brazilian highlands and north-east (NE) Brazil (Figures 16a and 16b). In Rio De Janeiro and São Paulo, 15-20% of the total extremes occur for 2 days consecutively (Figure 16a). From 1965–2004, the number of consecutive 2- and 3-days extremes show increasing trends in NE Brazil, few parts of the Brazilian Highlands and east Brazil including São Paulo but they decrease in Rio De Janeiro (Figures 16c and 16d). In Brasilia, the number of consecutive 2-days and 3-days extremes vary 20-25% and 6-8%, respectively, and they show decreasing trends from 1965–2004 (Figure 16).

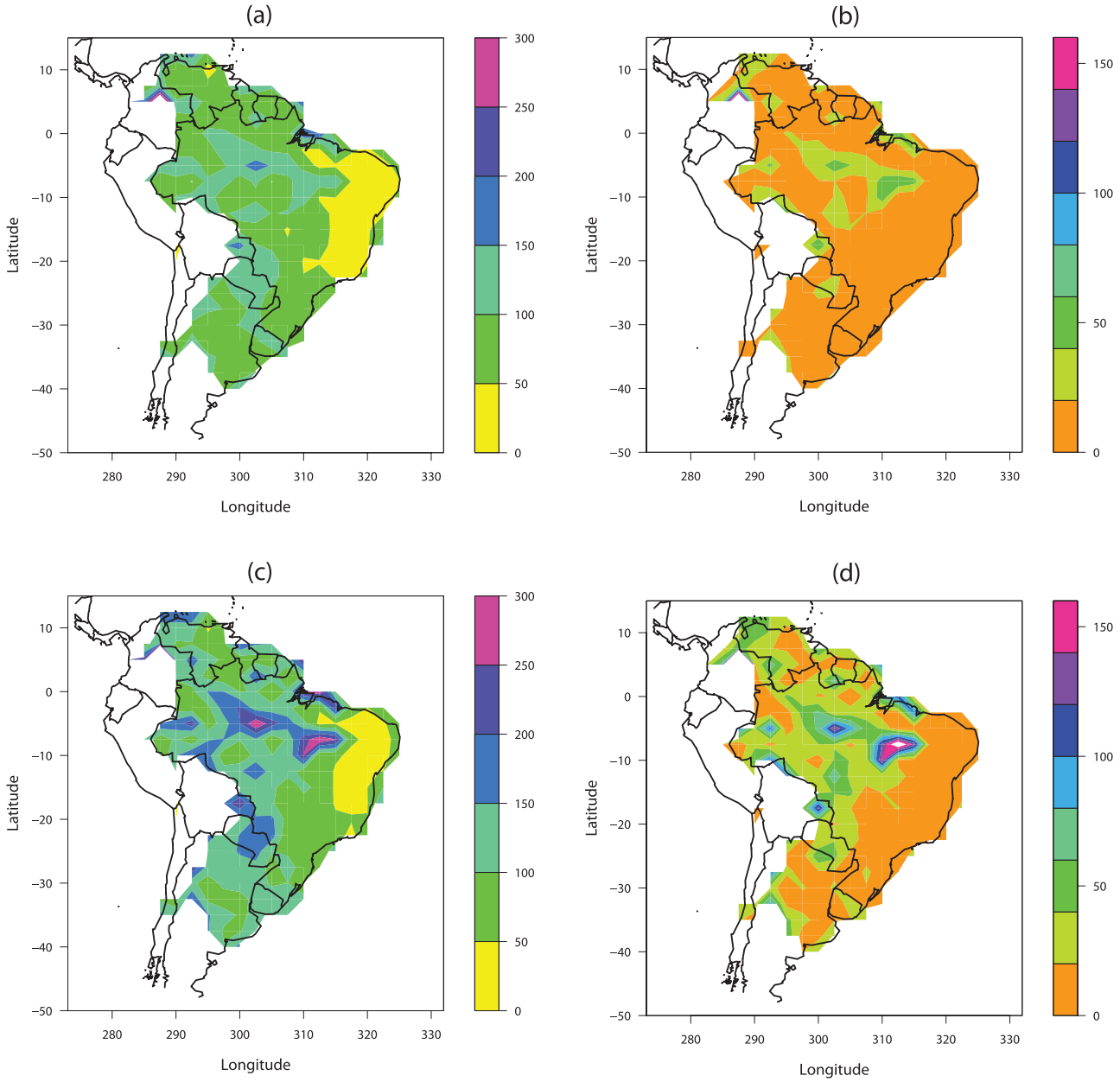

Figure 13. Spatial variability of 50-a and 200-a RLs and their standard errors in mm from weekly maxima precipitation residuals for 1940–2004: (a) 50-a RL; (b) Standard errors of 50-a RL; (c) 200-a RL; and (d) Standard errors of 200-a RL. In (d), the white region at a location given by (*longitude*, *latitude*) as (312.5, −7.5) indicates 193.48 mm.

[27] The Amazon basin experiences most of the extremes from January to April with March being the month most prone to extremes while it receives most of the precipitation from December to May (Figure 17). The wetter months in NE Brazil and Catingas are from December to May but they receive most of the extremes from January to April with March receiving the highest number of extremes. The Mato Grosso Plateau experiences most extremes from December to February with January receiving the highest number of extremes. The Brazilian highlands and south-east (SE) Brazil receives most of the precipitation from November to April but the highest number of extremes are observed in the summer months, i.e., December to February, with January being the most critical with respect to the number of extremes.

3.2. North Argentina

[28] Some parts of NE Argentina including Buenos Aires have higher thresholds relative to the other parts of South America (Figure 9). From 1965–2004, increasing trends in threshold are observed in the major parts of north Argentina excluding Buenos Aires. 50-a and 200-a RLs do not show much variations and their trends from 1965–2004 show increasing behavior in the major parts excluding Buenos Aires (Figures 13 and 14). The PEVI ranges from 1.1-1.2 in the major parts but it also lies between 1.2 and 1.3 in some

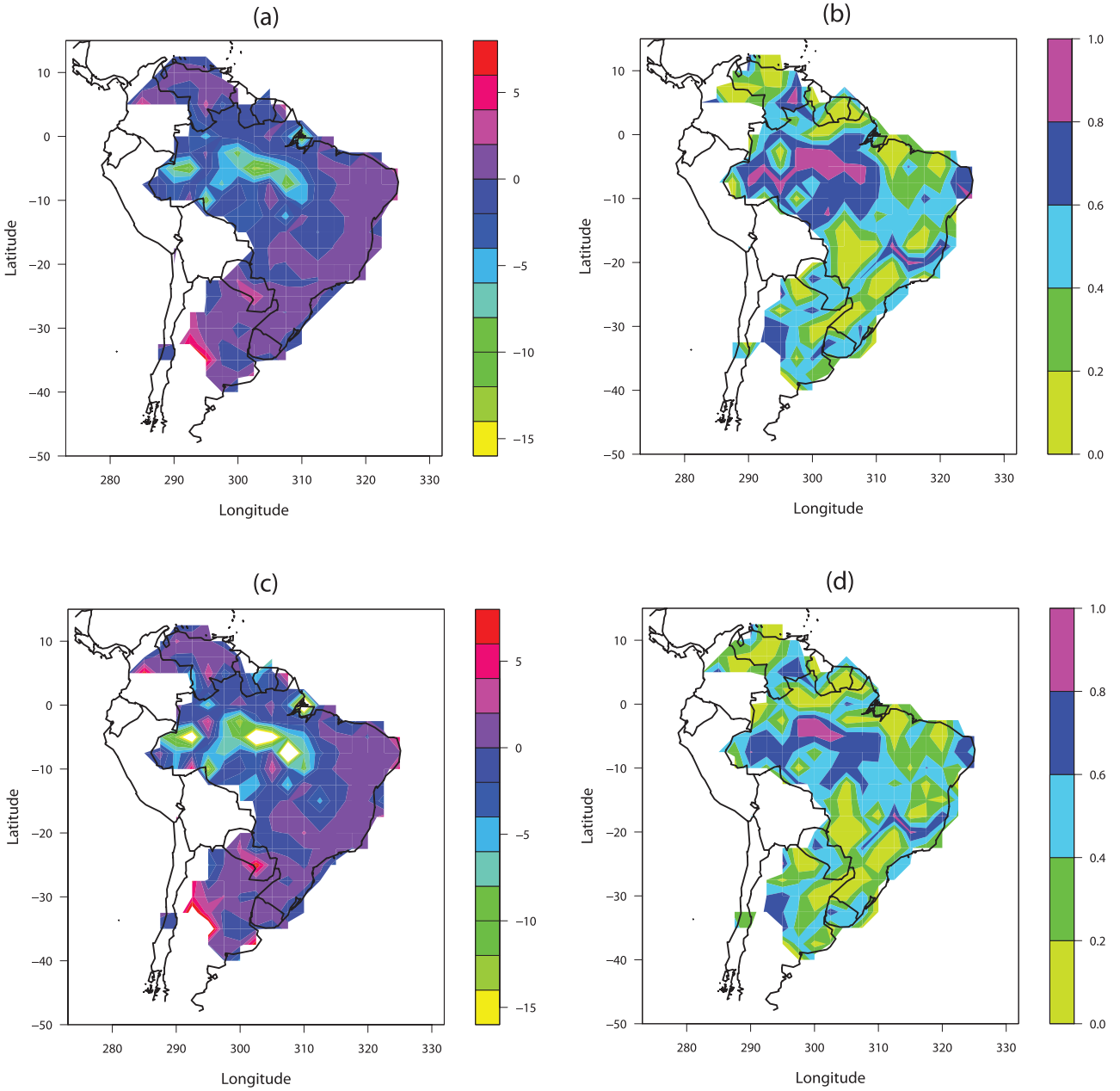

Figure 14. Temporal variability of 50-a and 200-a return levels (RL) from weekly maxima precipitation residuals for 1965–2004: (a) Temporal variability of 50-a RL from 1965–2004; (b) R^2 from linear trends shown in (a); (c) Temporal variability of 200-a RL from 1965–2004; and (d) R^2 from linear trends shown in (c). In (c), the white regions at four locations given by (*longitude*, *latitude*) as (292.5, −5), (302.5, −5), (305, −5) and (307.5, −7.5) indicate −22.07, −26.39, −21.12, and −34.47, respectively.

parts including Buenos Aires (Figure 15). Only some parts of north Argentina excluding Buenos Aires show increasing trends in PEVI from 1965–2004. Less than 10% of the total extremes occur consecutively for 2 days (Figure 16a). The number of consecutive 3-days extremes is zero everywhere except in Buenos Aires and its surrounding regions where it is less than 2% (Figure 16b). Increasing trends in consecutive 2-days extremes are observed in the major parts from 1965–2004 (Figure 16c). For consecutive 3-days extremes, most of the areas experiences either no trends because of zero consecutive 3-days extremes or decreasing trends from 1965–2004 (Figure 16d). From 1965–2004, Buenos Aires receives increasing and decreasing number of consecutive 2-days and 3-days extremes, respectively. Argentina receives most of the precipitation in the summer months, i.e., December to February, but it experiences most of the extremes in late summer and autumn, i.e., February to April, with March receiving the highest number of extremes (Figure 17).

3.3. Venezuela

[29] In Venezuela, thresholds are low but they show increasing trends from 1965–2004 everywhere except in

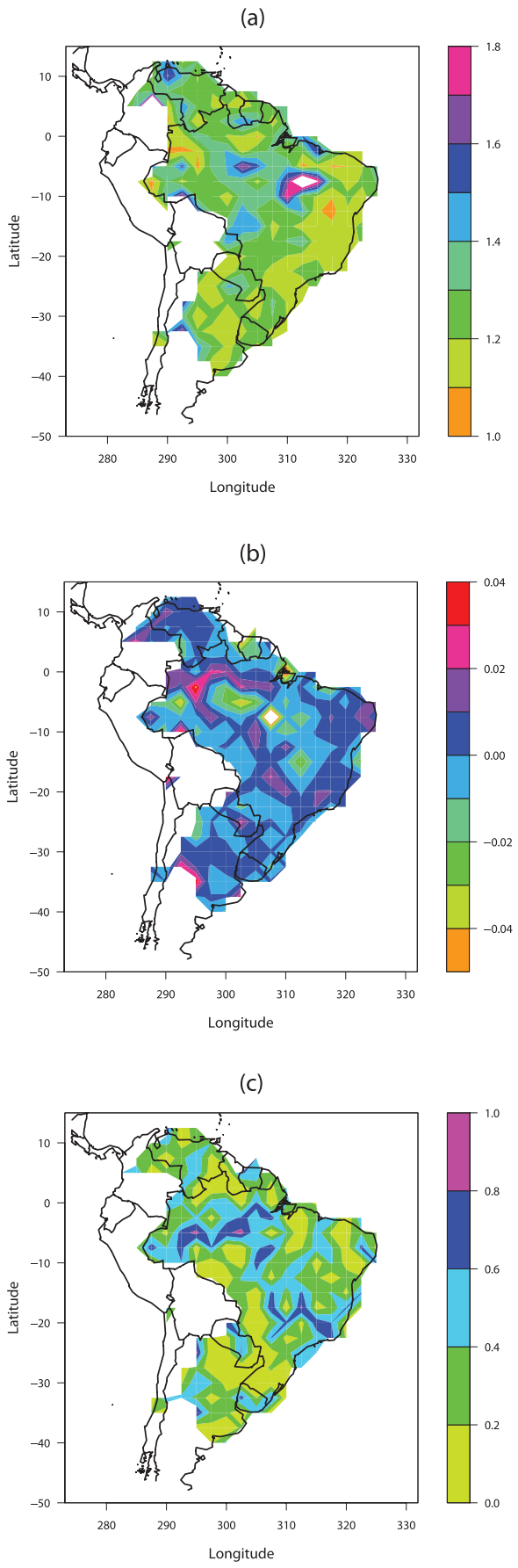

some southern parts (Figure 9). We do not observe much variations in 50-a and 200-a RLs but these RLs show increasing trends from 1965–2004 only in the northern parts including Caracas (Figures 13 and 14). The PEVI is between 1.2 and 1.3 everywhere except in NW including Caracas where it is high and ranges from 1.3-1.6 (Figure 15). Increasing trends in PEVI are observed from 1965–2004 in the major parts including Caracas. Some northern parts including Caracas receive 5–10% of the total extremes for 2 days consecutively (Figure 16a). Venezuela does not experience extremes occurring for 3 days consecutively (Figure 16b). From 1965–2004, the number of consecutive 2-days extremes shows increasing trends only in south Venezuela whereas no trends are observed in consecutive 3-days extremes in the major parts since these parts do not receive consecutive 3-days extremes (Figures 16c and 16d). Decreasing trends in consecutive 3-days extremes are observed from 1965–2004 only in east Venezuela. The main rainy season in Venezuela is from May to November and it receives the most number of extremes from June to August with June being the most critical with respect to the number of extremes (Figure 17).

3.4. Uruguay

[30] Uruguay has high thresholds in South America and their trends from 1965–2004 indicate increasing levels in the most parts except Montevideo and its surrounding regions (Figure 9). We do not observe much variations in 50-a and 200-a RLs and their trends show increasing behavior from 1965–2004 everywhere except in Montevideo and its surrounding areas (Figures 13 and 14). The PEVI ranges from 1.2-1.3 everywhere and it shows increasing trends from 1965–2004 in the whole country except Montevideo and its surrounding regions (Figure 15). 5–10% of the total extremes occur consecutively for 2 days whereas less than 2% of the total extremes occur for 3 days consecutively (Figures 16a and 16b). From 1965–2004, decreasing trends in the number of both consecutive 2- and 3-days extremes are observed (Figures 16c and 16d). Uruguay receives most of the precipitation in the autumn months, i.e., March to May, but the highest number of extremes are observed in April and October (Figure 17).

3.5. Paraguay

[31] In Paraguay, thresholds are high and they show increasing trends from 1965–2004 in most parts including Asuncion (Figure 9). 50-a RLs do not vary much whereas some variations are observed in 200-a RLs (Figure 13). Increasing trends in both 50-a and 200-a RLs are observed from 1965–2004 but these trends increase more rapidly in Asuncion and its surrounding areas as compared to the other parts (Figure 14). The PEVI varies from 1.1-1.3 everywhere

Figure 15. Precipitation extremes volatility index (PEVI), defined as the ratio of 200-a and 50-a RLs, from weekly maxima precipitation residuals: (a) Spatial variability for 1940–2004; (b) Temporal variability from 1965–2004; and (c) R^2 from linear trends shown in (b). In (a), the white regions at two locations given by (*longitude*, *latitude*) as (312.5, −7.5) and (315, −7.5) indicate 2.22 and 1.82, respectively. In (b), the white region at a location given by (*longitude*, *latitude*) as (307.5, −7.5) indicates 0.042.

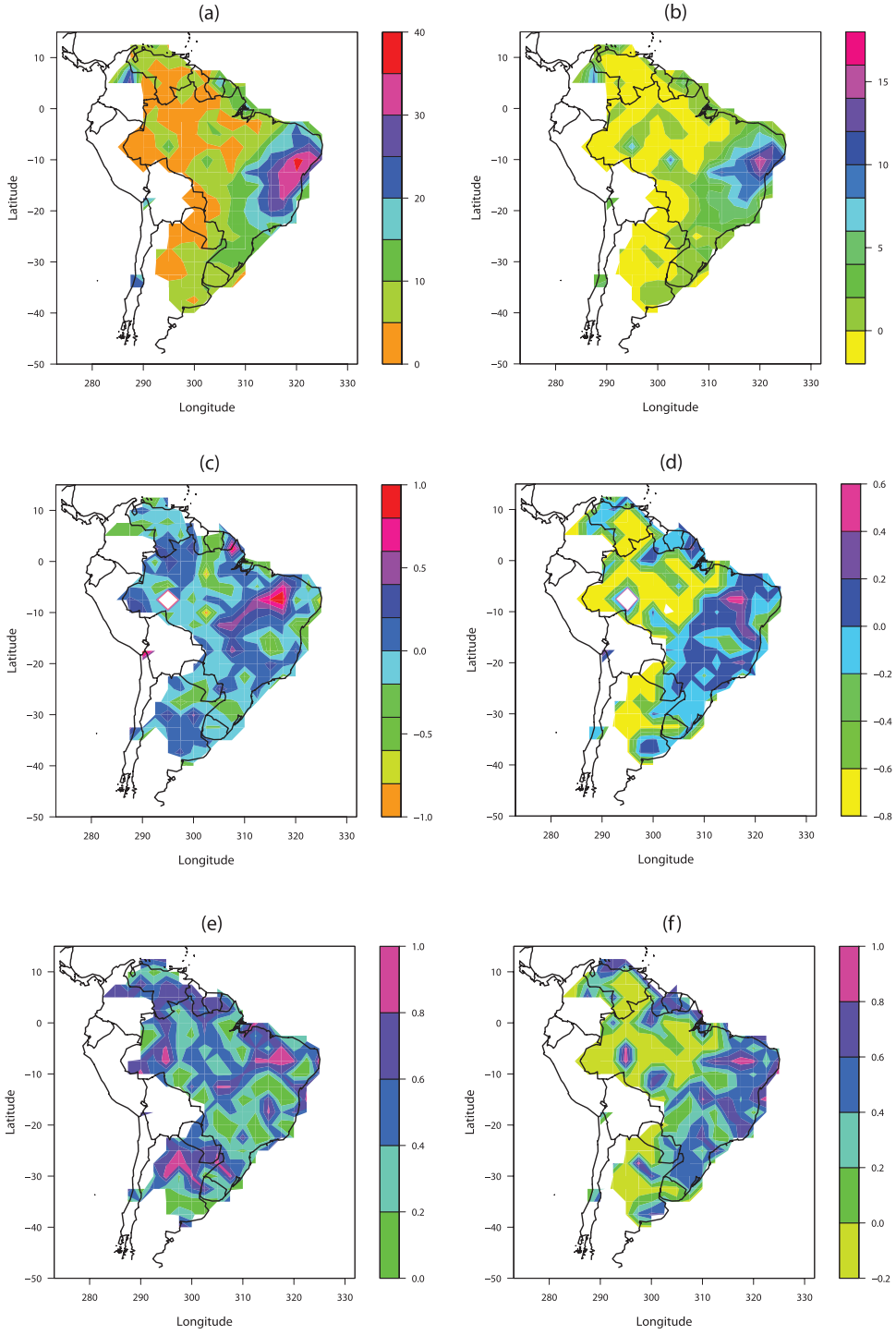

Figure 16. Percentage of the number of consecutive 2- and 3-days extremes out of the total number of extremes based on daily precipitation for 1940–2004. Threshold is chosen as the 99%-quantile of daily time series. (a) Spatial variability of consecutive 2-days extremes from 1940–2004; (b) Spatial variability of consecutive 3-days extremes from 1940–2004, where the yellow regions showing values between 0 and −2 do not indicate any values but represents regions where the number of consecutive 3-days extremes is zero; (c) Temporal variability of consecutive 2-days extremes from 1965–2004; (d) Temporal variability of consecutive 3-days extremes from 1965–2004, where the yellow regions showing values between -0.6 and -0.8 do not indicate any values but represents regions where the number of consecutive 3-days extremes is zero; (e) R^2 from linear trends shown in (c); and (f) R^2 from linear trends shown in (d), where the yellow regions that lies between 0 and -0.2 do not indicate R^2 values but represents grids where the number of consecutive 3-days extremes is zero. In (c), the white region at a location given by (*longitude*, *latitude*) as (295, −7.5) indicates 4.66. In (d), the white regions at two locations given by (*longitude*, *latitude*) as (295, −7.5) and (302.5, −10) indicate 4.71 and −0.97, respectively.

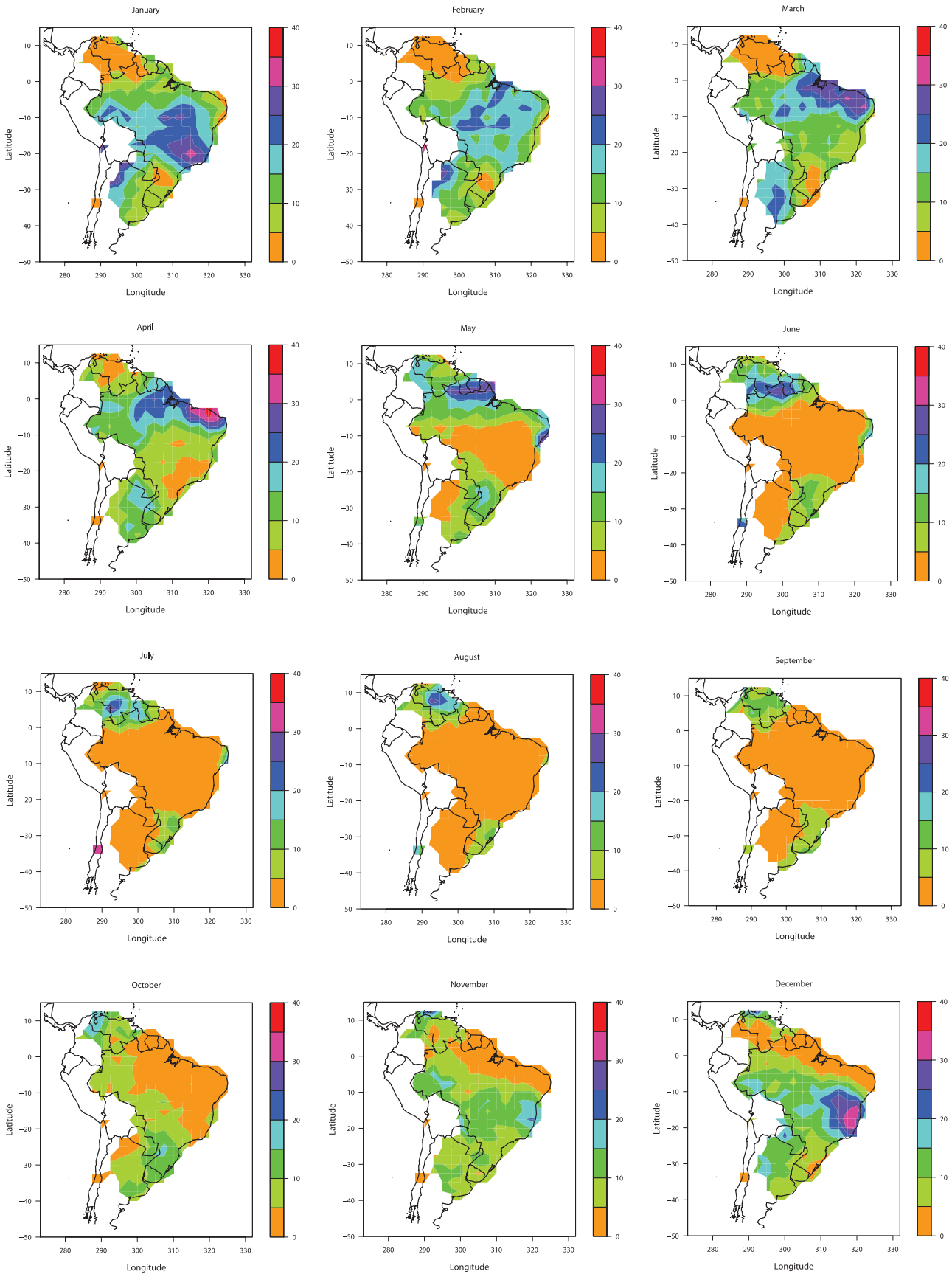
January
February
March
April
May
June
July
August
September
October
November
December
Latitude
Longitude
10
0
−10
−20
−30
−40
−50
280
290
300
310
320
330
40
30
20
10
0

Figure 17

except in Asuncion and its surrounding regions where it varies from 1.3–1.4 (Figure 15a). From 1965–2004, the PEVI increases in the major parts but it is increasing more rapidly in Asuncion and its surrounding areas as compared to the other parts (Figure 15b). The number of extremes occurring consecutively for 2 days is less than 10% of the total extremes whereas the major parts of the country do not receive consecutive 3-days extremes (Figures 16a and 16b). Decreasing trends in both consecutive 2- and 3-days extremes are observed from 1965–2004 (Figures 16c and 16d). In Asuncion, less than 5% and 2% of the total extremes occur for 2 and 3 days consecutively, respectively, and their trends show decreasing behavior from 1965–2004. Paraguay receives heavy precipitation in summer, i.e., October to March, and experiences the most number of extremes from December to February with December receiving the highest number of extremes (Figure 17).

3.6. Suriname and French Guiana

[32] In Suriname and French Guiana, thresholds are low but their trends from 1965–2004 show sharply increasing behavior everywhere including Paramaribo and Cayenne (Figure 9). No variations in 50-a and 200-a RLs are observed but trends in 50-a and 200-a RLs decrease in Suriname and increase in some parts of French Guiana including Cayenne (Figures 13 and 14). The PEVI lies between 1.2 and 1.4 in Suriname whereas it ranges from 1.2–1.3 in French Guiana (Figure 15a). From 1965–2004, the PEVI shows decreasing trends in both Suriname and French Guiana except Cayenne where the PEVI increases (Figure 15b). The number of consecutive 2-days extremes varies from 1–20% in Suriname with Paramaribo receiving 15-20% whereas it ranges from 10–15% in French Guiana (Figure 16a). Suriname receives less than 4% of the total extremes for 3-days consecutively with Paramaribo receiving 2–4% whereas in French Guiana, the number of consecutive 3-days extremes is less than 2% (Figure 16b). From 1965–2004, both consecutive 2- and 3-days extremes show decreasing trends in Suriname and increasing trends in the major parts of French Guiana including Cayenne (Figures 16c and 16d). Suriname receives heavy precipitation from April to August and experiences most of the extremes from April to June with May being the most critical with respect to the number of extremes (Figure 17). In French Guiana, the rainy season goes from April to July and the most intense months in terms of the number of extremes are from March to May with May receiving the highest number of extremes (Figure 17).

3.7. Extremes With Topography and Vegetation

[33] In mid- and high-altitudes of the Brazilian highlands and east Venezuela, the PEVI varies from 1.1–1.4 and shows increasing trends from 1965–2004 in some areas (Figure 15a). The high-altitudes of the Brazilian Highlands receive 20–35% and 6–16% of the total extremes consecutively for 2 and 3 days, respectively, and their trends show increasing behavior from 1965–2004 in some parts (Figure 16). However, in the high-altitudes of east Venezuela, consecutive 3-days extremes are not observed and less than 5% of the total extremes occur consecutively for 2 days and its trends show decreasing behavior from 1965–2004. The mid-altitudes and lowlands of east Brazil indicate very less variations in PEVI which lies between 1.1 and 1.2 but most of the eastern Brazil, which includes Rio De Janeiro and São Paulo, experience increasing trends in PEVI from 1965–2004 (Figure 15). In east Brazil, the number of consecutive 2- and 3-days extremes range from 10–30% and 1–14%, respectively, and their trends show increasing behavior from 1965–2004 only in some parts including São Paulo (Figure 16). Catingas with lowlands has the highest PEVI in South America whereas the lowlands of the Amazon basin and the Mato Grasso Plateau have higher PEVI values (Figure 15a). In the lowlands of Venezuela, north Argentina, Uruguay, Paraguay, Suriname, and French Guiana, the PEVI lies between 1.1 and 1.3 (Figure 15a). From 1965–2004, the major parts of the lowlands of the Amazon basin, north Venezuela, north Argentina, Uruguay, and Paraguay experience increasing trends in PEVI whereas decreasing trends in PEVI are observed in the lowlands of the Mato Grasso Plateau, Suriname, and French Guiana except Cayenne (Figure 15b). All the lowlands regions of Brazil, north Argentina, Venezuela, Paraguay, Uruguay, Suriname and French Guiana experience less than 10% of the total extremes for 2 days consecutively whereas the number of consecutive 3-days extremes is zero in most of these areas (Figures 16a and 16b). Only some of the lowlands areas of the Amazon basin particularly western parts of the basin, the Mato Grasso Plateau, south Venezuela, and north Argentina experience increasing number of consecutive 2-days extremes from 1965–2004 (Figure 16c).

[34] In the evergreen forests of the Amazon basin, south Venezuela, Suriname, and French Guiana, the PEVI ranges from 1.1–1.3 (Figure 15a). Catingas with evergreen forest has the highest PEVI in South America. Increasing trends in PEVI are observed only in some parts of the Amazon basin and south Venezuela (Figure 15b). In the Amazon basin, Catingas, and south Venezuela, the number of consecutive 2-days extremes is less than 10% of the total extremes and its trends show increasing behavior from 1965–2004 (Figures 16a and 16c). In Suriname, the number of consecutive 2-days extremes varies from 1-20% and shows decreasing trends from 1965–2004 whereas it ranges from 10–15% and indicates increasing trends from 1965–2004 in French Guiana. The number of consecutive 3-days extremes is zero in the evergreen forests of Catingas, south Venezuela, and some parts of the Amazon basin and shows decreasing trends in Suriname and increasing trends in the major parts of French Guiana from 1965–2004 (Figures 16b and 16d). In the savannas of north Venezuela, the PEVI ranges from 1.2–1.6 and shows increasing trends from 1965–2004 while the number of consecutive 2-days extremes is less than 10% and shows decreasing trends from 1965–2004 (Figures 15 and 16). In the cropland/

Figure 17. Percentage of the number of monthly extremes out of the total number of extremes based on daily precipitation for the period 1940–2004. Threshold is chosen as the 99%-quantile of daily time series. Extremes mostly occur from December to April with January receiving the highest number of extremes. The period from July to October is relatively quieter with respect to extremes.

natural vegetation of the Brazilian highlands, the Mato Grasso Plateau, east Brazil, north Argentina, Uruguay, and Paraguay, the PEVI is low and lies between 1.1 and 1.3 and shows increasing trends from 1965–2004 in some of their areas (Figure 15). The Brazilian highlands and NE Brazil experience 20-35% and 6-16% of the total extremes consecutively for 2 and 3 days, respectively, and their trends show increasing behavior from 1965–2004 in some areas (Figure 16). Less than 10% of the total extremes occur consecutively for 2 days in the Mato Grasso Plateau, SE Brazil, north Argentina, Uruguay, and Paraguay but their trends increase from 1965–2004 in some parts of the Mato Grasso Plateau and north Argentina. The number of consecutive 3-days extremes is less than 2% in SE Brazil, some parts of the Mato Grasso Plateau, north Argentina, Uruguay, and Paraguay. From 1965–2004, trends in consecutive 3-days extremes decrease in SE Brazil, the Mato Grasso Plateau, Uruguay, Paraguay but increase in some parts of north Argentina.

[35] A caution should be exercised while interpreting the results at all those grid points where $\overline{D}_{SP}$ is greater than one since at these grid points, we reject with 95% confidence that the inter-arrival times of threshold excesses follow a *homogeneous Poisson process*. The variability of extremes needs to be interpreted with care in view of issues like spatiotemporal variability in the quality of the observations as well as the possible influence of geographical features, atmospheric conditions, climate teleconnections and other phenomena that have not been considered in this study. The insights on the spatial and temporal variability of extremes will probably be more relevant in a comparative sense and at aggregate space-timescales rather than for the extremal analysis of individual points or for understanding localized phenomena related to extremes.

4. Summary and Conclusions

[36] This study analyzed the spatial and temporal variability of precipitation extremes in South America based on daily precipitation data available in 2.5° gridded fields from 1940–2004. At each grid point, 65 a of data from 1940–2004 were used to understand spatial variability whereas the temporal variability was investigated for 40 a (1965–2004) and was given as the slope of linear trend obtained by fitting a regression line to 16 values computed from 25-a moving window from 1965–2004, i.e., 1965–1989, 1966–1990,..., 1980–2004. We analyzed weekly precipitation maxima residuals and utilized the Poisson-GP model to investigate the spatial and temporal variability of threshold, the scale (σ) and shape (ξ) parameters, and 50-a and 200-a RLs. The temporal variability of precipitation were evaluated from the temporal variability of thresholds. The threshold was chosen as the 95%-quantile of time series. We also investigated the spatial and temporal variability of the PEVI, which measures the variability of extremes and is defined as the ratio of 200-a and 50-a RLs. On the basis of daily precipitation data, we investigated the spatial and temporal variability of the percentage of the number of consecutive 2- and 3-days extremes out of the total number of extremes. The spatial variability of the percentage of the number of extremes in a particular month out of the total number of extremes was also investigated based on daily precipitation data. The threshold for the analysis of daily precipitation data was chosen as the 99%-quantile of time series.

[37] Precipitation is high indicated by high thresholds in SE Brazil, Uruguay, Paraguay, and Buenos Aires. The PEVI is high in the eastern parts of the Amazon basin, Catingas, Mato Grasso Plateau, NW Venezuela including Caracas, and Asuncion. From 1965–2004, both precipitation and the PEVI show increasing trends in the eastern coastal regions of Brazil including Rio De Janeiro, the Brazilian highlands particularly southern parts, north Venezuela including Caracas, some parts of north Argentina, Uruguay, Paraguay including Asuncion, and Cayenne. The Amazon basin except eastern parts and São Paulo experience increasing trends in the PEVI and decreasing trends in precipitation. In the eastern parts of the Amazon basin, Catingas, the Mato Grasso Plateau, Brasilia, Buenos Aires, and Montevideo, simultaneous decreasing trends are observed in precipitation and the PEVI. The PEVI shows decreasing trends in Suriname including Paramaribo and French Guiana excluding Cayenne although increasing precipitation trends are observed in these areas. The number of consecutive 2- and 3-days extremes are high in the Brazilian Highlands, NE Brazil, and Brasilia. Trends in precipitation and the number of both consecutive 2- and 3-days extremes increase in few parts of the Brazilian Highlands and some parts of French Guiana including Cayenne. Catingas and some parts of east Brazil including São Paulo experience increasing trends in the number of consecutive 2- and 3-days extremes and decreasing trends in precipitation. The precipitation shows increasing trends whereas the number of consecutive 2- and 3-days extremes show decreasing trends in NE coastal regions of Brazil, Rio De Janeiro, Uruguay, Paraguay including Asuncion, and Suriname including Paramaribo. In Brasilia, both precipitation and the number of consecutive 2- and 3-days extremes show decreasing trends simultaneously. The number of consecutive 2-days extremes also show increasing trends in the Amazon basin particularly western parts, some parts of the Mato Grasso Plateau, and Buenos Aires although precipitation shows decreasing trends in these areas. Simultaneous decreasing trends are observed in precipitation and the number of consecutive 3-days extremes in the Mato Grasso Plateau and Buenos Aires from 1965–2004.

[38] The areas of interest based on an increasing PEVI from 1965–2004, are the Amazon basin, the Brazilian Highlands, Venezuela, Uruguay, Paraguay, and some of the highly populated cities in South America, specifically Rio De Janeiro, São Paulo, Caracas, Asuncion, and Cayenne. Some parts of east Brazil, few parts of the Brazilian highlands, São Paulo, and Cayenne also experience increasing number of consecutive 2- and 3-days extremes. Water resources engineers and planners, disaster management agencies, and policy makers need to pay special attention to the regions with increasing trends in the PEVI and consecutive 2- and 3-days daily extremes, especially when these regions overlap with densely populated areas, while planning for infrastructure development and disaster management. Civil engineers can utilize the results of this study for the design of hydraulic structures, specifically when considering the optimal safety factors in their design. Hydrologists and climatologists need to delve deeper into

the potential causes of the observed spatiotemporal trends in extremes for delineating the variability of extremes due to natural and anthropogenic effects.

[39] Precipitation extremes may result in significant loss of human life and property. However, the damages caused by precipitation can be influenced by a variety of factors other than just precipitation maxima or the statistical properties thereof. These factors include surface and sub-surface hydrology since the damages caused by precipitation extremes are primarily caused by floods and flash floods, which, in turn, are strongly influenced by the physics of runoff and infiltration. The other factor is population: certainly the (catastrophic) impact of disasters depends on (high) population densities and the location of critical infrastructures or national/human assets which may be potentially damaged by precipitation extremes. Finally, the actual damages would also be a function of resilience of communities and critical infrastructures to precipitation extremes and related disasters.

[40] Future research needs to explore the use of extreme value theory in conjunction with more advanced physically based or statistical models of precipitation, as well as the utilization of emerging techniques for the estimation of the extreme value parameters directly as a function of time, seasonality and other covariates. In addition, development of heuristic approaches for the estimation of optimal thresholds in the context of precipitation data may need to be explored, since similar approaches developed for other types of data may or may not be directly applicable to precipitation data, especially when the data sets are large. Hydrologists and climatologists can perform further research based on this study to understand the natural or anthropogenic causes driving precipitation extremes and their spatial or temporal trends. Future research may combine the PEVI used in this study with other factors like population and critical infrastructures to estimate the potential risks from extremes and subsequently with development or financial indices to estimate the corresponding impacts.

[41] **Acknowledgments.** This research was funded by the SEED of the Laboratory Directed Research and Development (LDRD) Program of the Oak Ridge National Laboratory (ORNL), managed by UT-Battelle, LLC for the U.S. Department of Energy under Contract DE-AC05- 00OR22725. We would like to gratefully acknowledge Dave Allured and Brant Liebmann from the NOAA-CIRES Climate Diagnostics Center, Boulder, Colorado, for providing us the data set used in this study. The authors are thankful to two anonymous reviewers for their helpful suggestions which significantly improved the quality of the paper. Shiraj Khan would like to acknowledge the help and support provided by Prof. Sunil Saigal of the Civil and Environmental Engineering at the University of South Florida. Auroop R. Ganguly would like to thank Dr. Rick Katz of the National Center for Atmospheric Research and Prof. Tailen Hsing of the Ohio State University for their help and support with the SEED project.

References

Brown, B. G., and R. W. Katz (1995), Regional analysis of temperature extremes: Spatial analog for climate change?, *J. Clim.*, *8*, 108–119.

Brunetti, M., M. Maugeri, T. Nanni, and A. Navarra (2002), Droughts and extreme events in regional daily Italian precipitation series, *Int. J. Climatol.*, *22*, 543–558.

Carvalho, L. M. V., C. Jones, and B. Liebmann (2002), Extreme precipitation events in southeastern South America and large-scale convective patterns in the South Atlantic Convergence Zone, *J. Clim.*, *15*, 2377–2394.

Cavazos, T. (2000), Using self-organizing maps to investigate extreme climate events: An application to wintertime precipitation in the Balkans, *J. Clim.*, *13*, 1718–1732.

Coles, S. G. (1989), On goodness-of-fit tests for the two-parameter Weibull distribution derived from the stabilized probability plot, *Biometrika*, *76*(3), 593–598.

Coles, S. G. (2001), *An introduction to statistical modeling of extreme values*, Springer-Verlag, London, UK.

Curriero, F. C., J. A. Patz, J. B. Rose, and S. Lele (2001), The association between extreme precipitation and waterborne disease outbreaks in the United Status, 1948–1994, *Am. J. Public Health*, *91*, 1194–1199.

Easterling, D. R., J. L. Evans, P. Y. Groisman, T. R. Karl, K. E. Kunkel, and P. Ambenje (2000), Observed variability and trends in extreme climate events, *Bull. Am. Meteorol. Soc.*, *81*, 417–425.

Gaines, S. D., and M. W. Denny (1993), The largest, smallest, highest, lowest, longest, and shortest: Extremes in ecology, *Ecology*, *74*, 1677–1692.

Galambos, J. (1987), *The asymptotic theory of extreme order statistics*, Robert E. Krieger, Malabar, Florida, USA.

Goswami, B. N., V. Venugopal, D. Sengupta, M. S. Madhusoodanan, and P. K. Xavier (2006), Increasing trend of extreme rain events over India in a warming environment, *Science*, *314*, 1442–1445.

Groisman, P. Y., et al. (1999), Changes in the probability of heavy precipitation important indicators of climatic change, *Climatic Change*, *42*, 243–283.

Gumbel, E. J. (1958), *Statistics of extremes*, Columbia Univ. Press, New York.

Haylock, M., and C. Goodess (2004), Interannual variability of European extreme winter rainfall and links with mean large-scale circulation, *Int. J. Climatol.*, *24*, 759–776.

Hellstrom, C., and B. A. Malmgren (2004), Spatial analysis of extreme precipitation in Sweden 1961–2000, *AMBIO: A J. Human Environment*, *33*, 187–192.

Iwashima, T., and R. Yamamoto (1993), A statistical analysis of the extremes events: Long-term trend of heavy daily precipitation, *J. Meteorol. Soc. Jpn.*, *71*, 637–640.

Jenkinson, A. F. (1955), The frequency distribution of the annual maxima (or minima) values of meteorological elements, *Q. J. Meteorol. Soc.*, *81*, 158–171.

Karl, T. R., R. W. Knight, and N. Plummer (1995), Trends in high-frequency climate variability in the twentieth century, *Nature*, *377*, 217–220.

Katz, R. W. (2002), Stochastic modeling of hurricane damage, *J. Appl. Meteorol.*, *41*, 754–762.

Katz, R. W., M. B. Parlange, and P. Naveau (2002), Statistics of extremes in hydrology, *Adv. Water Resour.*, *25*, 1287–1304.

Katz, R. W., G. S. Brush, and M. B. Parlange (2005), Statistics of extremes: Modeling ecological disturbances, *Ecology*, *86*(5), 1124–1134.

Kimber, A. C. (1985), Tests for the exponential, Weibull and Gumbel distributions based on the stabilized probability plot, *Biometrika*, *72*(3), 661–663.

Li, Y., W. Cai, and E. P. Campbell (2005), Statistical modeling of extreme rainfall in southwest western Australia, *J. Clim.*, *18*, 852–863.

Liebmann, B., and D. Allured (2005), Daily precipitation grids for South America, *Bull. Am. Meteorol. Soc.*, *86*(11), 1567–1570.

Liebmann, B., C. Jones, and L. M. V. Carvalho (2001), Interannual variability of daily extreme precipitation events in the state of São Paulo, Brazil, *J. Clim.*, *14*, 208–218.

Manton, M. J., et al. (2001), Trends in extreme daily rainfall and temperature in southeast Asia and the south Pacific: 1961–1998, *Int. J. Climatol.*, *21*, 269–284.

Meehl, G. A., and C. Tebaldi (2004), More intense, more frequent, and longer lasting heat waves in the 21st century, *Science*, *305*, 994–997.

Michael, J. R. (1983), The stabilized probability plot, *Biometrika*, *70*(1), 11–17.

Nadarajah, S. (2005), Extremes of daily rainfall in west central Florida, *Climatic Change*, *69*, 325–342.

Palutikof, J. P., B. B. Brabson, D. H. Lister, and S. T. Adcock (1999), A review of methods to calculate extreme wind speeds, *Meterological Applications*, *6*, 119–132.

Peterson, T. C., et al. (2002), Recent changes in climate extremes in the Caribbean region, *J. Geophys. Res.*, *107*(D21), 4601, doi:10.1029/2002JD002251.

Picklands, J. (1975), Statistical inference using extreme order statistics, *Ann. Stat.*, *3*, 119–131.

Rajagopalan, B., and U. Lall (1999), A k-nearest-neighbor simulator for daily precipitation and other weather variables, *Water Resour. Res.*, *35*(10), 3089–3101.

Schoenberg, F. P., R. Peng, and J. Woods (2003), On the distribution of wildfire sizes, *Environmetrics*, *14*, 583–592.

Stedinger, J. R., and T. A. Cohn (1986), Flood frequency analysis with historical and paleoflood information, *Water Resour. Res.*, *22*(15), 785–793.

Suppiah, R., and K. J. Hennessy (1998), Trends in total rainfall, heavy rainfall events, and number of dry events in Australia, *Int. J. Climatol.*, *18*, 1141–1164.

Todorovic, P., and E. Zelenhasic (1970), A stochastic model for flood analysis, *Water Resour. Res.*, *6*, 1641–1648.

Wilson, P. S., and R. Toumi (2005), A fundamental probability distribution of heavy rainfall, *Geophys. Res. Lett.*, *32*, L14812, doi:10.1029/2005GL022465.

Yates, D., S. Gangopadhyay, B. Rajagopalan, and K. Strzepek (2003), A technique for generating regional climate scenarios using a nearest-neighbor algorithm, *Water Resour. Res.*, *39*(7), 1199, doi:10.1029/2002WR001769.

D. J. Erickson III and G. Ostrouchov, Computer Science and Mathematics Division, Oak Ridge National Laboratory, Oak Ridge, TN 37831, USA.

A. R. Ganguly, S. Khan, and G. Kuhn, Computational Sciences and Engineering Division, Oak Ridge National Laboratory, 1 Bethel Valley Rd., Oak Ridge, TN 37831, USA. (gangulyar@ornl.gov)